EUROPEAN COMMISSION

Community Research

SEVENTH FRAMEWORK PROGRAMME

CARBOWASTE

Treatment and Disposal of Irradiated Graphite and Other Carbonaceous Waste

Grant Agreement Number: FP7-211333

Preliminary Report (T-4.4.1)
- 14 C Reduction in Graphite and spent Fuel Matrix -

Author(s): K. Baginski, D. Vulpius, W.von Lensa
Forschungszentrum Juelich, IEF-6

Date of issue of this report : 25/03/2010

Project co-funded by the European Commission under the Seventh Framework Programme (2007 to 2011) of the European Atomic Energy Community (EURATOM) for nuclear research and training activities		
Dissemination Level		
PU	Public	
RE	Restricted to the partners of the CARBOWASTE project	
CO	Confidential, only for specific distribution list defined on this document	**X**

Start date of project : **01/04/2008** Duration : **48 Months**

Distribution list

Person and organisation name and/or group	Comments
WP3 & WP4 Partners	

CARBOWASTE		
Work package: 4 **Task: :** 4.4	**CARBOWASTE document no:** CARBOWASTE-1006-T-4.4.1	**Document type:** T=Technical Report
Issued by: FZJ, Germany **Internal no.:** CW1006-T-4-4-1		**Document status:** Draft

Document title

^{14}C Reduction in Graphite and spent Fuel Matrix

Executive summary

The report provides a first compilation of experiments performed at the research centre Juelich on thermal and chemical treatment of irradiated graphite.

The investigated material is taken from the thermal column of the Juelich MERLIN MTR and from broken pieces of HTR fuel pebbles and the AVR reflector.

The results show that ^{14}C can be released in a much higher fraction than the associated mass loss of the samples.

The process parameters still need to be optimized.

Tritium can practically totally be extracted at higher treatment temperatures.

The report will be further accomplished when new results will be available.

Revisions

Rev.	Date	Short description	Author	Internal Review	Task Leader	WP Leader
00	Dd/mm/yyyy	Issue	Name, Organisation	Name, Organisation *Signature*	Name, Organisation *Signature*	Name, Organisation *Signature*
01	01/06/2010	First issue	Baginski	Von Lensa	Vulpius	
02	yy/xx/2010	2nd Issue				

1.1 List of Content

1.1 List of Content 4
1.2 List of tables 5
1.3 List of figures 7
2 Introduction and objectives 9
3 Statement of problem 10
3.1 Graphite in nuclear technology 10
3.1.1 Graphite structure 10
3.1.2 Chemical reactions of carbon 11
3.1.3 Graphite in reactor core structure 13
3.2 Graphite waste management 16
3.2.1 Nature of radionuclide contamination 16
3.2.2 Diffusion of radionuclides in graphite 18
3.2.3 Reprocessing of contaminated graphite 21
4 Experimental part 24
4.1 Equipment 24
4.2 Reagents and investigated materials 24
4.3 Performance of experiments 25
5 Results and discussion 29
5.1.1 Treatment in argon atmosphere 29
5.1.2 Oxidation with water steam 31
5.1.3 Release rates 35
5.1.4 Migration of other radionuclides during graphite thermal treatment 45
6 Summary and outlook 47
7 References 49
8 Appendix 54

1.2 List of tables

Table 1. Approximate relative rates of gas-carbon reactions at 800°C and 0.1 atm pressure ... 13

Table 2. Concentrations of impurities in AVR graphite ... 16

Table 3. Activation reactions producing ^{14}C ... 17

Table 4. Total radioactivity in AVR graphite ... 18

Table 5. Diffusion coefficients of nuclear graphite ... 21

Table 6. Radioactive graphite treatment in argon atmosphere ... 25

Table 7. Radioactive graphite treatment in water steam atmosphere ... 25

Table 8. Oxidation of Merlin graphite powder at increasing temperature ... 25

Table 9. Diffusion coefficients of tritium in Merlin and AVR graphite ... 39

Table 10. Results of γ- and total γ, β-activity measurements of Merlin graphite samples ... 45

Table 11. Radionuclide distribution after treatment of AVR graphite in argon atmosphere ... 46

Table 12. Radionuclides distribution after treatment of AVR graphite in water steam (water vapour pressure 31 kPa) ... 46

Table 13. Tritium and ^{14}C release from Merlin graphite massive sample, 870°C, argon ... 54

Table 14. Tritium and ^{14}C release from Merlin graphite powder sample, 970°C, argon ... 55

Table 15. Tritium and ^{14}C release from Merlin graphite powder sample, 1050°C, argon ... 56

Table 16. Tritium and ^{14}C release from Merlin graphite massive sample, 1060°C, argon ... 57

Table 17. Tritium and ^{14}C release from AVR graphite powder sample, 1060°C, argon ... 58

Table 18. Tritium and ^{14}C release from Merlin graphite powder sample, 960°C, p_{H2O} 7.4 kPa, flow rate 80 ml/min ... 59

Table 19. Tritium and ^{14}C release from Merlin graphite powder sample, 960°C, p_{H2O} 7.4 kPa, flow rate 660 ml/min ... 60

Table 20. Tritium and ^{14}C release from Merlin graphite massive sample, 1060°C, p_{H2O} 2.3kPa ... 61

Table 21. Tritium and ^{14}C release from Merlin graphite powder sample, 1050°C, p_{H2O} 2.3 kPa ... 62

Table 22. Tritium and ^{14}C release from Merlin graphite powder sample, 1060°C, p_{H2O} 7.4 kPa, flow rate 660 ml/min ... 63

Table 23. Tritium and ^{14}C release from AVR graphite powder sample, 1060°C, 2.3 kPa ... 64

Table 24. Tritium and ^{14}C release from AVR graphite powder sample, 1060°C, p_{H2O} 31 kPa ... 65

Table 25. γ-analysis of AVR graphite 66
Table 26. γ-analysis of Merlin graphite 66

1.3 List of figures

Figure 1. The crystal structure of hexagonal graphite 11

Figure 2. Ideal reaction zones in graphite: I – reaction rate is controlled by chemical reactivity of the sample; II – reaction rate is controlled by diffusion in pores; III – reaction rate is controlled by gas transport to the exterior surface of the sample; a and b – transition zones 12

Figure 3. AVR graphite and carbon installations..... 14

Figure 4. The major processing steps in the production of a conventional polygranular carbon 15

Figure 5. Atom movement in crystal lattice: a) jump to neighbouring vacancies or interstitial position, b) exchange of atoms 19

Figure 6. The porous structure of graphite..... 20

Figure 7. Graphite treatment scheme 23

Figure 8. Washing procedure of reactor tube..... 26

Figure 9. Installation for graphite thermal treatment 28

Figure 10. Tritium release in argon atmosphere 29

Figure 11. ^{14}C release from AVR and Merlin graphite in argon 30

Figure 12. Tritium release with step-by-step temperature increase by oxidation in water steam vapour pressure 70 kPa 31

Figure 13. a - tritium release from Merlin graphite powder during oxidation at saturated water vapour pressure 7.4 kPa; b - tritium release from Merlin and AVR graphite at 1060°C and saturated water vapour pressure 2.3 kPa 32

Figure 14. ^{14}C release with step-by-step temperature increase by oxidation in water steam vapour pressure 70 kPa 33

Figure 15. ^{14}C release (a) and mass loss (b) during Merlin graphite oxidation with water steam (water vapour pressure 7.4 kPa)..... 34

Figure 16. ^{14}C release (a) and mass loss (b) during Merlin and AVR graphite oxidation with water steam (water vapor pressure 2.3 kPa) 35

Figure 17. Release rates and released amounts of ^{14}C, ^{12}C and ^{3}H from Merlin graphite oxidised in water steam at 1060°C and water vapour pressure 2.3 kPa..... 36

Figure 18. Ratio of normalised release rates of ^{3}H to ^{12}C in inert atmosphere..... 37

Figure 19. Model of hydrogen trapping sites in a graphite material..... 37

Figure 20. Microstructural models of isotropic and anisotropic graphite..... 38

Figure 21. Tritium release vs. square root of the treatment time 39

Figure 22. Arrhenius plot for tritium diffusion in Merlin graphite 40

Figure 23. Ratio of normalised release rates of ^{14}C to ^{12}C in inert atmosphere 41

Figure 24. Ratio of normalised release rates of ^{3}H to ^{12}C in oxidising atmosphere 42

Figure 25. Ratio of normalised release rates of ^{14}C to ^{12}C in oxidising atmosphere 43

Figure 26. ^{14}C release vs. fractional release of ^{12}C during treatment in different conditions (MM – Merlin graphite massive sample, MP – Merlin graphite powder) 44

Figure 27. ^{3}H release vs. fractional release of ^{12}C during treatment in different conditions (MM – Merlin graphite massive sample, MP – Merlin graphite powder) 45

Figure 28. CO and CO_2 concentration in the outlet of carrier gas, Merlin graphite powder sample, 970°C, argon 55

Figure 29. CO and CO_2 concentration in the outlet of carrier gas, Merlin graphite powder sample, 1050°C, argon 56

Figure 30. CO and CO_2 concentration in the outlet of carrier gas, Merlin graphite massive sample, 1060°C, argon 57

Figure 31. CO and CO_2 concentration in the outlet of carrier gas, AVR graphite powder sample, 1060°C, argon 58

Figure 32. CO and CO_2 concentration in the outlet of carrier gas 59

Figure 33. CO and CO_2 concentration in the outlet of carrier gas, Merlin graphite powder sample, 960°C, p_{H2O} 7.4 kPa, flow rate 660 ml/min 60

Figure 34. CO and CO_2 concentration in the outlet of carrier gas, from Merlin graphite massive sample, 1060°C, p_{H2O} 2.3kPa 61

Figure 35. CO and CO_2 concentration in the outlet of carrier gas, Merlin graphite powder sample, 1050°C, p_{H2O} 2.3 kPa 62

Figure 36. CO and CO_2 concentration in the outlet of carrier gas, Merlin graphite powder sample, 1060°C, p_{H2O} 7.4 kPa, flow rate 660 ml/min 63

Figure 37. CO and CO_2 concentration in the outlet of carrier gas, AVR graphite powder sample, 1060°C, 2.3 kPa 64

Figure 38. CO and CO_2 concentration in the outlet of carrier gas, AVR graphite powder sample, 1060°C, p_{H2O} 31 kPa 65

2 Introduction and objectives

Graphite has been widely used as a moderator, reflector and fuel matrix in various types of nuclear reactors. At the end of reactor life activated graphite and carbon installations are radioactive waste, which requires a special waste management strategy.
The direct disposal in deep geological formations is one of the most probable ways of radioactive graphite management. However, the large volume of contaminated graphite reduces significantly the cost efficiency of this management route. For example, in case of AVR decommissioning 67 Mg of reflector graphite and 158 Mg of carbon isolation represents a great volume of low and medium active radioactive waste. This graphite contains significant quantities of radionuclides from neutron activation of impurities and contamination with fission products. Reprocessing of the graphite offers the opportunity to separate the majority of the short-lived isotopes from graphite. Thereafter only a small active residue fraction has to be disposed and the main mass of graphite can be reused.
The proposed purification procedure is based on the graphite gasification. This procedure allows to separate non-volatile and volatile radionuclides by chemical methods. The CO_2 formed can be released to atmosphere or precipitated as carbonates. The chemical methods are not capable to separates the carbon isotopes: long-lived radioactive ^{14}C and non-radioactive ^{12}C. In principle, the off gases from incineration can be fractionated in order to recover ^{14}C by isotope separation. However, the development of simplified method for graphite purification from ^{14}C would give an additional economical benefit.
The main objective of the present work was to investigate the influence of high temperature treatment on the release of radioactive carbon and other radionuclides from contaminated graphite.

3 Statement of problem

3.1 Graphite in nuclear technology

The properties of graphite make it suitable for many nuclear applications. By far the greatest use has been as moderator and reflector, because nuclear graphite has an absorption cross section for thermal neutrons as low as 3.5 to 3.8 mb. Furthermore, graphite is strong enough to serve as a structural component, eliminating the necessity of employing metals with higher cross sections.
The high-temperature strength, stability, and thermal conductivity of graphite make it good for use in high temperature reactors as a matrix material for ceramic fuels such as the uranium oxides and carbides.
In the reactor core boronated graphite is sometimes used as a high-temperature control-rod material. Designs for gas-cooled reactors employ graphite sleeves that support the fuel elements and channel the coolant. Also it is useful as a container for reactor irradiation experiments.

3.1.1 Graphite structure

Pure graphite is one of the most chemically inert materials. It is resistant to most acids, alkalis and corrosive gases. The crystallographic structure has a considerable influence on the chemical reactivity of graphite.
The basis of the crystal structure of graphite is the graphene plane of carbon layer plane, i.e. an extended hexagonal array of carbon atoms with sp^2 σ bonding and delocalised π bonding. The most common crystal form of graphite is hexagonal and consists of a stack of layer planes in the stacking sequence ABABAB.**.**The rhombohedral form of graphite with a stacking sequence ABCABC is a minor component of well-crystallised graphite. The theoretical density of both forms of graphite is 2.26 g/cm^3; the in-plane C-C distance is 0.142 nm and the interlayer distance 0.335 nm. Such a difference results from different types of chemical bonding. The usual assumption is that interlayer potentials are of van der Waals type. The bond strength within the layer planes is approximately 150 kcal/(gram atom), whereas the interlayer binding energy is estimated to be 1.3 kcal/(gram atom).
The structure given on Figure 1 is a perfect crystal structure of graphite. Solid carbons, in general, are less perfect. They constitute of domains of carbon atoms arranged in hexagonal pattern but these domains vary in degree of ordering and in value of interlayer space. Interlayer spacing is larger than for the graphite crystal (up to 0.344 instead of 0.335 nm). The most disordered carbons have so called “turbostratic” structure when carbon layer planes oriented randomly about c-axis.
Pyrolitic carbon has such a structure, usually with many warped basal planes, lattice defects and crystallite imperfection.

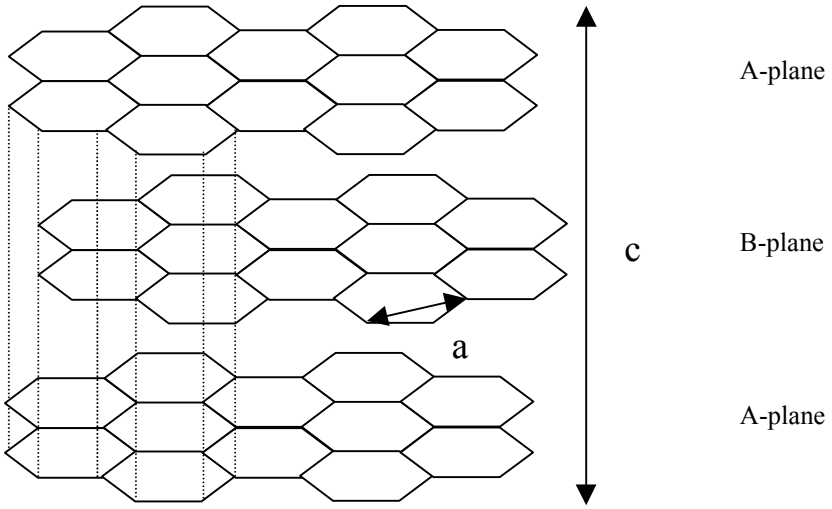

Figure 1. The crystal structure of hexagonal graphite

The anisotropy of the graphite crystal leads to different physical properties and chemical reactivity in different crystallographic directions. The energy of prismatic plane amounts 5 J/m^2 and 0.11 J/m^2 for basal plane, so reactions take place preferably at the edges (prismatic surface) and at defect sites.
As it was shown by Laine and co-workers [1] the different reactivity of carbon materials can be ascribed to the fact that different carbons have, initially, different amounts of active surface area. Graphite materials with large crystals and few defects have the best chemical stability.

3.1.2 Chemical reactions of carbon

3.1.2.1 Gas-phase reactions

At room temperature graphite does not react with gases like O_2, CO_2, H_2O and H_2. Above 400°C these gases start reacting with graphite. The temperature, at which reaction takes place, depends on the perfection of the graphite's crystal structure.
Heterogeneous reactions involving a porous solid and a gas can be controlled by one or more of three idealised steps:

1. Mass transport of the reacting gas from gas stream to the exterior graphite surface.
2. Mass transport of the reacting gas from the exterior surface to an active sites and mass transport of the products in the opposite direction.
3. Chemical reaction at the active sites.

The variation of reaction rate with temperature for gas-carbon reactions can be divided into tree main zones Figure 2.
In the low temperature zone I, the reaction is controlled by the chemical reactivity of the solid (step 3). There will be almost no concentration gradient of reacting gases throughout the whole volume of the sample due to low reaction rate, and this provides a uniform access to all the interior surface of porous material. For graphite - oxygen reaction the upper limit for temperature will be 500°C, for graphite-steam system - 850°C [2].

In the intermediate-temperature zone (zone II), step 2 becomes important. The diffusion of reactants in pores will influence the oxidation rate of material. At higher temperatures the concentration gradient of the reacting gas becomes steeper within graphite and the gas concentration becomes zero at a distance *R* nearer the surface. The activation energy E_a in this zone amounts ½ from true activation energy E_t. For graphite-water steam reaction this temperature region is characterised by temperature 850-1350°C and graphite oxygen reaction 500-900°C.
In the high temperature zone (>900°C for graphite oxygen and >1250-1400°C for graphite-water steam) - zone III - the concentration of the reacting gas is low at the exterior of the solid and the rate is controlled by the step 1. Since bulk gas-transfer processes have low activation energies, the apparent activation energy for gas-carbon reactions in zone III is low.

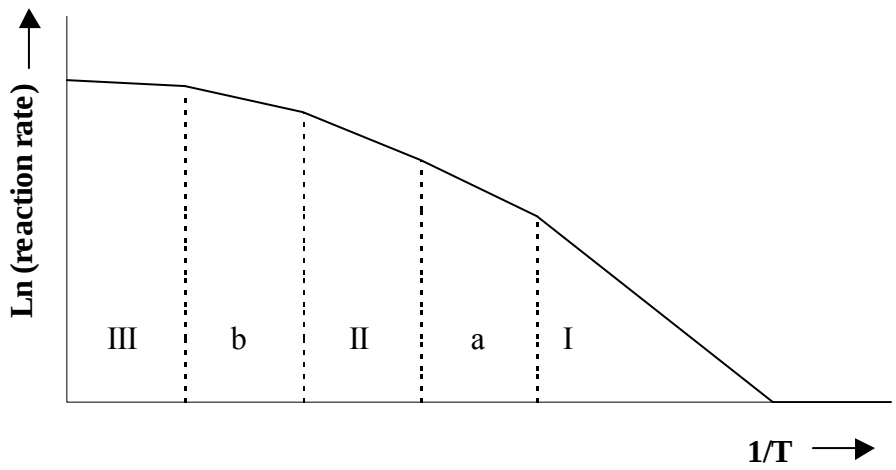

Figure 2. Ideal reaction zones in graphite: I – reaction rate is controlled by chemical reactivity of the sample; II – reaction rate is controlled by diffusion in pores; III – reaction rate is controlled by gas transport to the exterior surface of the sample; a and b – transition zones

The reactions occurring in the gas-graphite system are:

Reactions with oxygen

$C(s) + O_2(g) \rightarrow CO_2(g)$	$\Delta H = -394.5$ kJ/mol	Eq. (1)
$C(s) + 1/2O_2(g) \rightarrow CO(g)$	$\Delta H = -110.5$ kJ/mol	Eq. (2)
$CO(g) + 1/2O_2(g) \rightarrow CO_2(g)$	$\Delta H = -283.0$ kJ/mol	Eq. (3)

Where ΔH is the standard enthalpy of formation at 25°C. The above reactions are exothermic and favoured thermodynamically. But carbon does not readily react with air, so kinetic factors are obviously of importance.

Reaction with carbon dioxide

Boudouard reaction:

$C(s) + CO_2(g) \rightarrow 2CO$	$\Delta H = +172.5$ kJ/mol	Eq. (4)

The equilibrium can be shifted with increasing of CO pressure [3, 4] or in the presence of catalyst.

Reaction with water

$C(s) + H_2O(g) \rightarrow CO(g) + H_2(g)$ $\Delta H = + 131.3$ kJ/mol Eq. (5)

$CO(g)+H_2O(g) \rightarrow CO_2(g) + H_2(g)$ $\Delta H = - 213.7$ kJ/mol Eq. (6)

The hydrogen and CO_2 produced can then react with carbon

$C + CO_2(g) \rightarrow 2CO(g)$ $\Delta H = +172.5$ kJ/mol Eq. (4)

$C + H_2(g) \rightarrow CH_4(g)$ $\Delta H = -71.81$ kJ/mol Eq. (7)

The presence of hydrogen can shift reaction Eq. (5) left [4].

Reaction with hydrogen

$C + H_2(g) \rightarrow CH_4(g)$ $\Delta H = -71.81$ kJ/mol Eq. (7)

The mechanism and kinetics of these reaction are described by Walker [5].
The approximate relative rates of gas-carbon reactions at 800°C and 0.1 atm are given at Table 1.

Table 1. Approximate relative rates of gas-carbon reactions at 800°C and 0.1 atm pressure

Reaction	Relative rate
$C\text{-}O_2$	$1x10^5$
$C\text{-}H_2O$	3
$C\text{-}CO_2$	1
$C\text{-}H_2$	$3x10^{-3}$

There are a number of investigations of the nuclear graphite reactivity in different oxidation conditions in literature. Results of oxidation of HTR-10 nuclear graphite IG-11 [6] exhibited three regimes: 400-600°C with activation energy of 158.56 kJ/mol, 600-800°C where the activation energy was 72.05 kJ/mol and „third-zone“ over 800°C regime with very low oxidation energy. The comparison of reactivity of two types of graphite used in HTR in oxygen and air at 650-900°C (regime II) makes a conclusion that there is no difference in behaviour of matrix graphite (A3-27) and standard graphite V483T during oxidation [7]. In the same time at lower temperature (400°C, regime I) matrix graphite is more reactive in respect to air. For temperature range 350-520°C activation energy E_a for A3-3 graphite matrix amounts to 110 kJ/mol [8].

3.1.3 Graphite in reactor core structure

3.1.3.1 Design of AVR core structure

The reactor core of AVR represents a cylindrical vessel made of high-purity graphite of 50 cm wall thickness which serves as reflector [9] Figure 3. The graphite brick reflector vessel is enclosed in a 50 cm envelope made from carbon bricks (graphite with larger amounts of

impurities), which provides shielding and heat isolation. All this composition is surrounded by double wall steel liner. The bottom and top reflector also consist of graphite and carbon bricks. The reflector of the AVR is made of the graphite quality ARS/AMT produced by the Sigri-Company [10]. This graphite is based on the needle coke and densified by extruding which leads to high anisotropy.

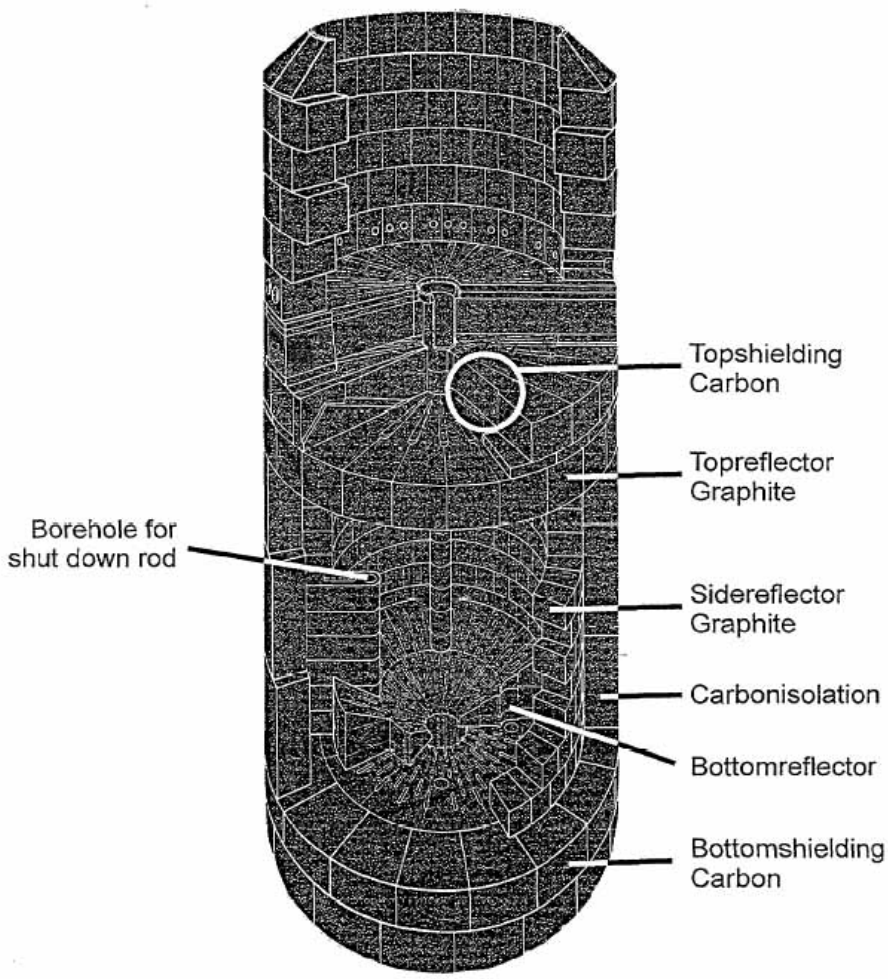

Figure 3. AVR graphite and carbon installations

3.1.3.2 Nuclear graphite manufacture

The major processing steps in the manufacture of reflector graphite are summarised in Figure 4. Detailed procedure is described in [11].

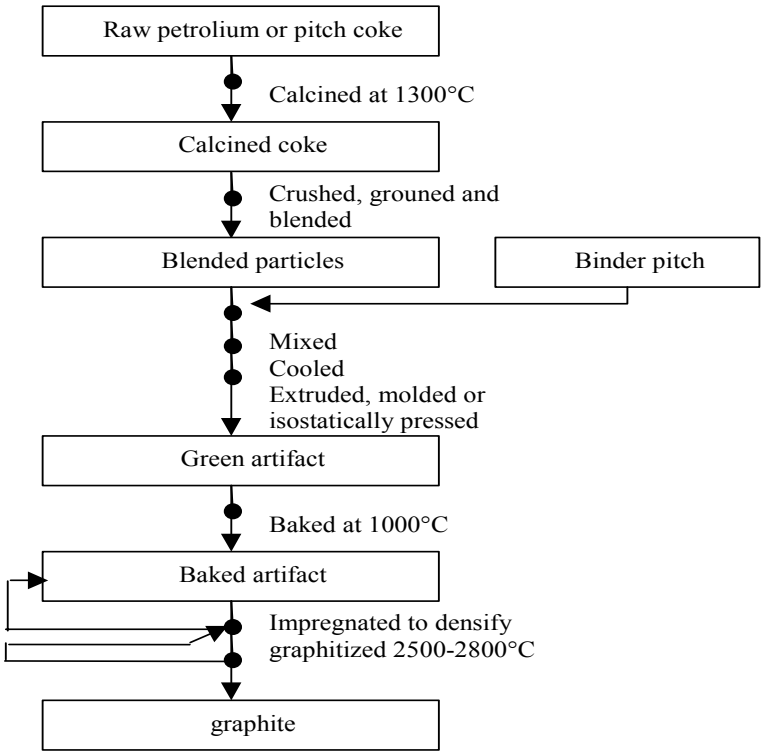

Figure 4. The major processing steps in the production of a conventional polygranular carbon

Polygranular graphite consists of two phases: a filler material and a binder pitch. European nuclear graphites are typically made from a coal-tar pitch-derived coke. The coke is usually calcined at 1300°C before it will be crushed and blended. The binder phase is coal-tar pitch. The binder plasticizes the filler coke particles so that they can be formed. Commonly used forming processes include extrusion, moulding, and isostatic pressing. The binder phase is carbonised during the subsequent baking operation (~1000°C). Frequently, engineering graphites are pitch impregnated to densify the carbon artifact, followed by rebaking. The final stage of the manufacturing process is graphitisation (2500-3000°C) during which carbon atoms in the baked material migrate to form the thermodynamically more stable graphite lattice. Nuclear graphites require high chemical purity to minimise neutron adsorption and activation of impurities. Also certain elements catalyse the oxidation of graphite and must be reduced to an acceptable level. This is achieved by selecting very pure cokes, utilising a high graphitisation temperature (>2800°C), or by including a halogen purification stage in the manufacture of the cokes or graphite. All low-boiling point impurities will be removed by graphitisation. Impurities that remain are those which form carbides or are soluble in graphite. For example vanadium carbide has a melting point in excess of 2800°C; boron carbide melts at 2350°C but also forms a substitutional impurity in the graphite lattice, which is extremely stable.

3.2 Graphite waste management

3.2.1 Nature of radionuclide contamination

Radioactivity in graphite and carbon/slag results from the neutron capture reaction on carbon itself and on impurities like cobalt, iron, lithium, nitrogen, etc. In the case of AVR impurity concentration in reflector graphite and insulation layers of carbon bricks are different (Table 2). The other contributions to the total inventory of radionuclides in the graphite must be considered. Besides the activation of carbon and of stable impurities in the graphite these are the fission of natural uranium present in the graphite as an impurity and the possibility of primarily surface contamination from the other regions of the reactor.

Table 2. Concentrations of impurities in AVR graphite

Element	Concentration, ppm		Activation product
	Isolation carbon	Reflector graphite	
Li	30	2	^{3}H
B	10	2	^{3}H
C	9.90E+05	1.00E+06	^{14}C
N	4500	30	^{14}C
Cl	15	0.2	^{36}Cl
K	1600	30	^{40}K
Ca	1500	100	^{41}Ca
Fe	7000	1000	^{55}Fe
Co	10	0.2	^{60}Co
Ni	40	10	^{63}Ni
Nb	2.5	0.05	^{94}Nb
Mo	10	2	^{93}Mo, ^{99}Tc
Cs	1	0.01	^{134}Cs
Ba	100	20	^{133}Ba
Sm	2	0.02	^{151}Sm, ^{155}Eu
Eu	0.1	0.02	^{152}Eu, ^{154}Eu

Tritium

The radionuclide ^{3}H, tritium has a half-life time of 12.3 years. The contribution of radioactivity in nuclear graphite arising from tritium is significant [12-14]. It will be produced by the following reactions:

- Fission reaction, such as $^{235}U(n,f)\ ^{3}H$ reactions,
- $^{6}Li(n,\alpha)\ ^{3}H$ reactions, lithium presents as an impurity in the graphite matrix of the fuel element and in the reflector,
- $^{3}He\ (n,p)\ ^{3}H$ reactions of the ^{3}He isotope present in the helium coolant,
- $^{10}B\ (n,2\alpha)\ ^{3}H$ reactions in the absorber rods (negligible for designs without core rods).

Main contribution to accumulation of tritium in graphite is given by neutron reactions with ^{6}Li and ^{3}He nuclei. Tritium generated from lithium impurities present in graphite is mostly produced in graphite bulk. The release of tritium is controlled by its diffusion out of the grain boundaries and into the pore system.
The chemical properties of tritium are essentially the same as those of ordinary hydrogen. One of the most important reactions is isotopic exchange where tritium can substitute hydrogen atom in water molecule or in organic molecule. The exchange process

$$HT + H_2O \rightleftharpoons HTO + H_2 \qquad \text{Eq. (8)}$$

is rather slow at room temperature (equilibrium constant K=6 at 25°C) because the hydrogen in is tightly bound.

Radiocarbon

Radionuclide ^{14}C has a half-life time of 5730 years. It is mainly produced in the reactor graphite through following neutron reactions:

Table 3. Activation reactions producing ^{14}C

Reaction	Capture cross section in barns ($10^{-24}cm^2$)	Abundance of isotope in %
^{13}C (n, γ) ^{14}C	$0.9 \cdot 10^{-3}$	1.1 ^{13}C/carbon
^{14}N (n, p) ^{14}C	1.81	99.63 ^{14}N/nitrogen
^{17}O (n, a) ^{14}C	0.235	0.04 ^{17}O/oxygen

In the reactor core materials nitrogen is present only as an impurity, whereas carbon and oxygen are in some cases major constituent elements of the coolant, moderator or fuel. In spite of this fact, the ^{14}N activation reaction is usually the most important contributor to ^{14}C production because of its larger cross section and high isotopic abundance of ^{14}N in natural nitrogen. Nitrogen in graphite is in bound state, substituting for carbon atoms in nodes of crystal lattice, or in gaseous form filling pores in graphite. The kinetic energy of formed ^{14}C atom is about 470 kJ/mol. This value is equivalent to the bond energy between C-C bound and C=C bond. It was suggested [15] that the formed ^{14}C atom stays in the same position as ^{14}N locates. Thus the level and location of nitrogen impurity in all reactor core materials is an important parameter. The nitrogen levels vary widely from 10 to 100 ppm in different reactor graphites [16] and sometimes they are not known very precisely. It was shown that nitrogen content is the largest on the surface [15]. From surface to about 30 nm in depth, nitrogen concentration decreases.

Caesium

The three radioactive caesium isotopes ^{134}Cs, ^{135}Cs and ^{137}Cs are produced by nuclear fission and neutron capture reaction:

$^{235}U \rightarrow {}^{137}Cs, {}^{135}Cs$

$^{235}U \rightarrow {}^{133}Cs$ (n, γ) ^{134}Cs

^{134}Cs can be also produced from the stable isotope impurity during reaction:

^{133}Cs (n, γ) ^{134}Cs

The half-life of Cs isotopes is two year for ^{134}Cs, $2 \cdot 10^{6}$ for ^{135}Cs and 30.1 for ^{137}Cs. The sources of radioactive Cs contamination are: uranium impurities in reactor graphite, uranium

presenting in the circuit from fuel elements externally contaminated during manufacture, volatilisation of Cs from defective fuel due to its high vapour pressure. This Cs can be absorbed in graphite and form the interstitial compounds [17].

Europium

^{152}Eu, ^{154}Eu, ^{155}Eu are produced by fission reaction and their half-life amounts to 12.4 years, 8.5 years and 4.5 years. The isotopes can be also formed by activation of impurities ^{151}Eu, ^{153}Eu and ^{154}Sm.

Cobalt

Cobalt-60 originates from neutron activation of stable Co-59, which is present as an impurity in nuclear reactor graphite, and has a half-life 5.3 years.
The Table 4 shows the calculated total radioactivity in AVR graphite in the end of 1988 [18].

Table 4. Total radioactivity in AVR graphite

Radionuclide	Total radioactivity, Bq	
	Reflector graphite	Isolation carbon
^{3}H	8.8E+14	6.9E+15
^{14}C	4.6E+12	2.9E+14
^{36}Cl	1.5E+09	5.9E+10
^{41}Ca	5.8E+10	4.5E+11
^{55}Fe	1.1E+15	4.0E+15
^{60}Co	4.2E+13	1.1E+15
^{63}Ni	4.1E+12	8.5E+12
^{93}Mo	2.5E+08	4.1E+08
^{99}Tc	2.8E+07	3.5E+07
^{134}Cs	8.9E+11	3.1E+13
^{133}Ba	3.5E+11	7.1E+11
^{151}Sm,	4.5E+08	1.8E+10
^{152}Eu	1.4E+07	2.9E+07
^{154}Eu	1.5E+11	3.0E+11
^{155}Eu	6.3E+10	2.5E+12
^{166m}Ho	2.2E+09	4.3E+10

3.2.2 Diffusion of radionuclides in graphite

Diffusion can be defined as the mechanism by which matter is transported into or through matter.
In polycrystalline materials the mechanism of diffusion is very complex. Different types of diffusion are to be called depending upon the kind of the medium, which differ in the progressive motion of the atoms and in the rate of diffusion. The *volume diffusion* describes

progressive movement of atoms in a solid with regular lattice structure. The movement of atoms in crystals is possible mainly due to presence of different kinds of defects. Different motion possibilities exist for the lattice-own atoms as well as for foreign atoms [19] (Figure 5):

a) when atom is displaced from lattice site and jumps to neighbouring vacancies or interstitial position.

b) when exchange of lattice positions involving two, three or four atoms situated next to one another in the crystal structure.

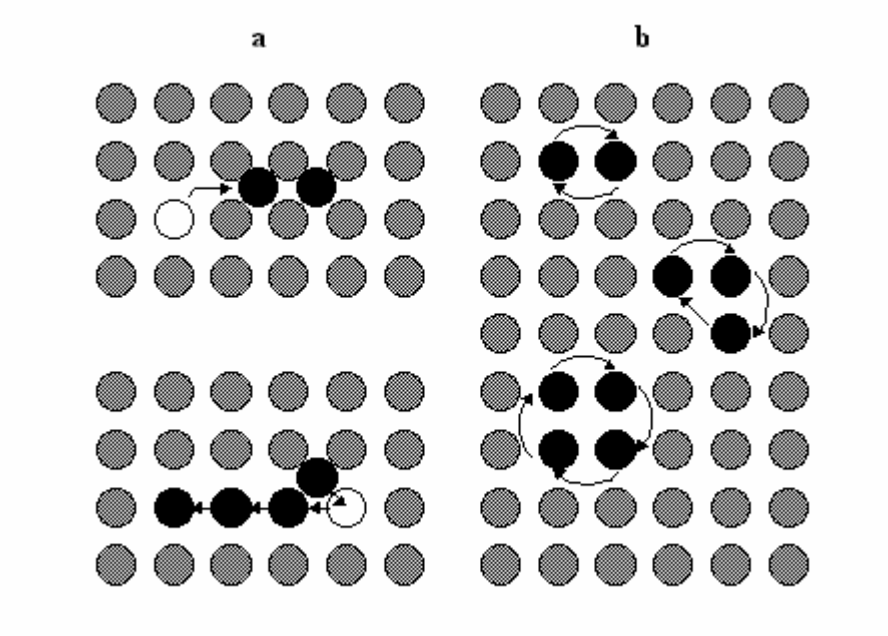

Figure 5. Atom movement in crystal lattice: a) jump to neighbouring vacancies or interstitial position, b) exchange of atoms

The other type of diffusion, connected with structure of solid substance, is the grain boundary diffusion. An illustration of the porous structure of graphite is shown in Figure 6. It consists of granules of size around a few microns with voids in between. The granules themselves are made up from small crystallites. The volume diffusion takes place inside these granules. The demarcation of grains from each other leads to free space, which together with grain surfaces is enclosed in the term the "grain boundaries". The rate of *diffusion along grain boundaries* is much faster than that of diffusion in the bulk crystal.

Pore diffusion plays a role in porous materials. If the diffusing atoms form the bond with grain surface, the mechanism of grain boundary diffusion will be valid. In the case of noble gases (Kr, Xe), when it is no chemical interaction with the surface of material, an unhindered transition of fission gases occurs from grains to pores. Then a free movement of the diffusing atoms is possible as in a gas. Therefore pore diffusion can be compared with diffusion gas phase.

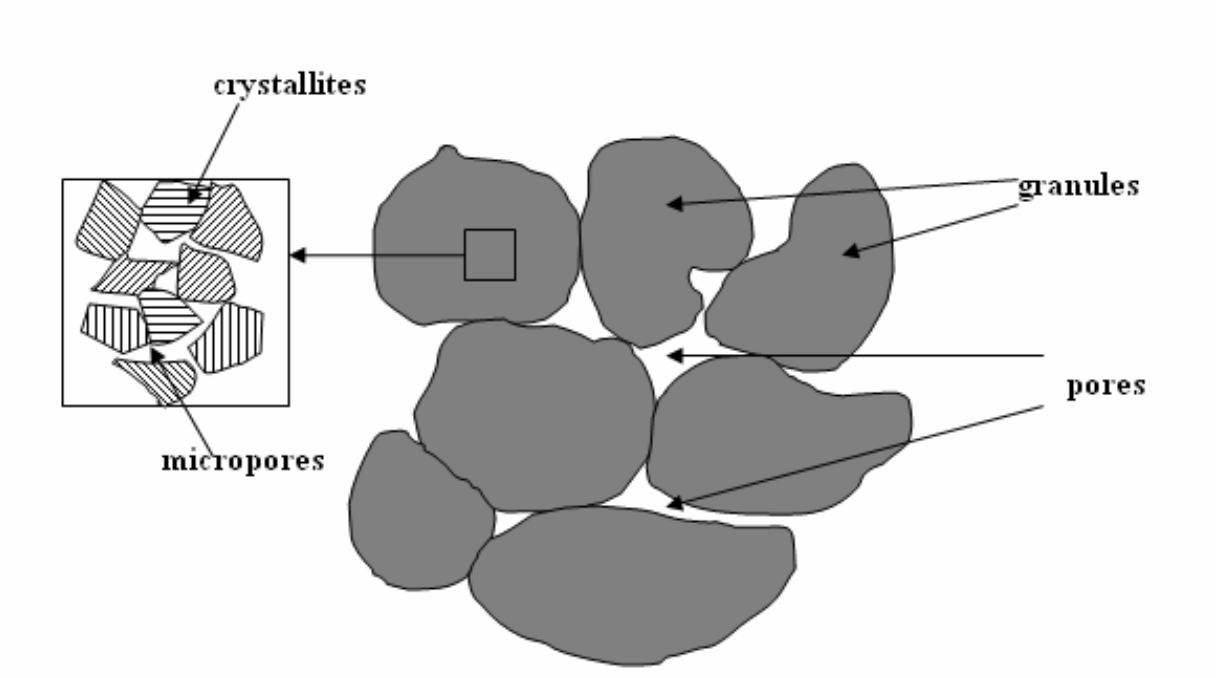

Figure 6. The porous structure of graphite

The behaviour of radionuclides in graphite at high temperatures is of great importance. It depends on the properties of diffusing substance. The temperature dependence of diffusion coefficient is expressed by Arrhenius equation:

$$D = D_0 e^{-\frac{E_a}{RT}} \qquad \text{Eq. (9)}$$

where D_0 – pre-exponential factor, E_a diffusion process activation energy.
Reduced diffusion coefficient D' (s^{-1}) is defined as the diffusion coefficient D (m^2/s) divided by the squared "equivalent sphere" diffusion radius, a (m):

$$D' = \frac{D}{a^2} \qquad \text{Eq. (10)}$$

The self-diffusion in graphite becomes essential above 2150°C. Diffusion coefficient was determined at 2200°C to be in the range $6.4 \cdot 10^{-20}$ to $3 \cdot 10^{-19}$ m^2/sec for different types of nuclear graphite [20].
Studies of the release behaviour of different radionuclides from graphite have been made. Diffusion coefficient for strontium in LTI-pyrocarbon (low temperature isotropic) varies from 10^{-12} to 10^{-8} cm^2/s in the temperature range 730 - 300°C. In graphite strontium diffusion is faster – diffusion coefficient amounts to 10^{-11} – 10^{-6} cm^2/s for the same temperature [21].
Caesium release from BISO coated particles is 32% after 1 hour of post-irradiation annealing at 2300°C, and europium release 23% after 3 hours [22]. In pyrocarbon layer caesium diffusion coefficient was $3 \cdot 10^{-8}$-$4 \cdot 10^{-11}$at the temperature 2200-1600 °C.
The experiments with irradiated BISO particles (FIMA 14%) showed that Sr and Cs were released at 2000°C after 5 hours almost quantitatively. Caesium released in amount of 72% and 26 % was retained in pyrocarbon layer. The release of Sr was about 92% [23].

Caesium is a very mobile element. During the procedure of graphite burning Cs can be released from graphite matrix, volatilised (Cs vapour pressure is 0.1 atm at 750°C) and transported from the furnace into the off-gas [12, 24]. The loss of Cs from graphite due to vaporisation was 15 % from total amount at 750°C after 9 hours of annealing [25]. The vaporisation of Sr and Ba from graphite body starts above 1200°C [25]. From 200 °C to 1200°C atoms of Ba move inside of graphite to active sites and can be leached out later.
Tritium emission from Windscale Pile I graphite was studied by Wörner et.al. [26]. After 30 min at 700 °C about 3% of the tritium was released.
Tritium behaviour in reactor graphite has been reported by Fischer and Malka [27, 28]. The reduced diffusion coefficient of tritium from pitch coke AS1-500, petroleum coke AL2-500 and graphite matrix A3-3 was determined (Table 5). The experiments were performed after irradiation of graphite in FRJ-1 (AS1-500 and A3-3) and AVR (AL2-500). In the first case the temperature during irradiation did not exceed 100°C (cold irradiation). In the case of AVR the irradiation temperature was about 500°C.
The diffusion process of tritium depends strongly on the nature of the graphite samples [29, 30]. As it was shown [30] the release behaviour depends strongly on the extent of graphite anisotropy and the diffusion of tritium in isotropic graphite will be faster than in anisotropic one.

Table 5. Diffusion coefficients of nuclear graphite

Type of graphite	Temperature, °C	Diffusion coefficient, D' s^{-1}
A3[1)]	800	1.72E-09
A3[1)]	850	9.09E-09
A3[1)]	900	6.89E-08
A3[2)]	1000	8.18E-09
AS1-500[2)]	1050	9.83E-11
AL2-500[2)]	1025	1.83E-10

1) - [28], 2) - [27]

3.2.3 Reprocessing of contaminated graphite

In the context of the final disposal route it is important to reduce waste volume. Processing of graphite by incineration offers the opportunity to separate the majority of graphite mass from the short-lived radioisotopes [31]. Only small residues (ash) remain for final storage. However, the release of ^{14}C in atmosphere accompanied with graphite burning is unfavourable. J.B. Mason and D. Bradbury [32] suggested to burn waste graphite without CO_2 release in environment. This methodology involved the use of pyrolysis/steam reforming followed by off-gas control. The exhaust gas could be solidified in the form of calcium carbonate, which could be used to fill voids in other radioactive waste. It was suggested that the process could either be used to process graphite removed from the core or even applied to gasify graphite waste within the core.

For conversion of carbon dioxide to an alkaline earth carbonate two options have been considered [33]. The first is direct precipitation:

$M(OH)_2 + CO_2 \rightarrow MCO_3 + H_2O$ Eq. (11)

(M = Ca, Sr or Ba).

The second alternative is the double alkali process. In the first step carbon dioxide is adsorbed by sodium hydroxide solution. The resulting sodium carbonate then reacts with an alkaline earth hydroxide in a separate vessel, to precipitate the carbonate and regenerate sodium hydroxide for recycle:

$2\ NaOH + CO_2 \rightarrow Na_2CO_3 + H_2O$ Eq. (12)

$Na_2CO_3 + M(OH)_2 \rightarrow 2\ NaOH + MCO_3$ Eq. (13)

However, reprecipitaion of carbon dioxide in carbonate form does not decide the problem of volume waste reduction. Moreover, carbonate wastes are less stable to leaching than graphite in elementary form. Dissolution rate of $CaCO_3$ reported in [34] amounts to $5.94 \cdot 10^{-7}$ mol/(cm^{2}day). For $MgCO_3$ it was found ~10^{-7} mol/(cm^{2}day) in the pH range 0-4 and ~10^{-9} mol/(cm^{2}day) in the pH range 5-8 [35]. Whereas graphite oxidation rate in pure water was determined as ~10^{-11} mol/(cm^{2}day) [36].

Carbon from gas phase can be precipitated in the form of elementary carbon as likely to be resistant to leaching. Contaminated graphite reacts with water steam in a fluidised bed with formation of CO. Elementary carbon can be obtained from Boudourd reaction from carbon monoxide:

$2\ CO \rightleftharpoons C + CO_2$ Eq. (4)

This reaction is exothermic from left to right. High conversion of carbon monoxide to carbon is possible in the presence of catalysis at relatively low temperature [37, 38]. The problem is that only half of carbon reacting will be immobilised as a solid. The other half (as carbon dioxide) would have to be recycled. The more preferred in this case is gasification of graphite with H_2 in order to methane formation. Subsequent pyrolysis of methane yields elementary carbon in form of soot.

The general scheme of graphite reprocessing with following separation of radionuclides is presented in Figure 7.

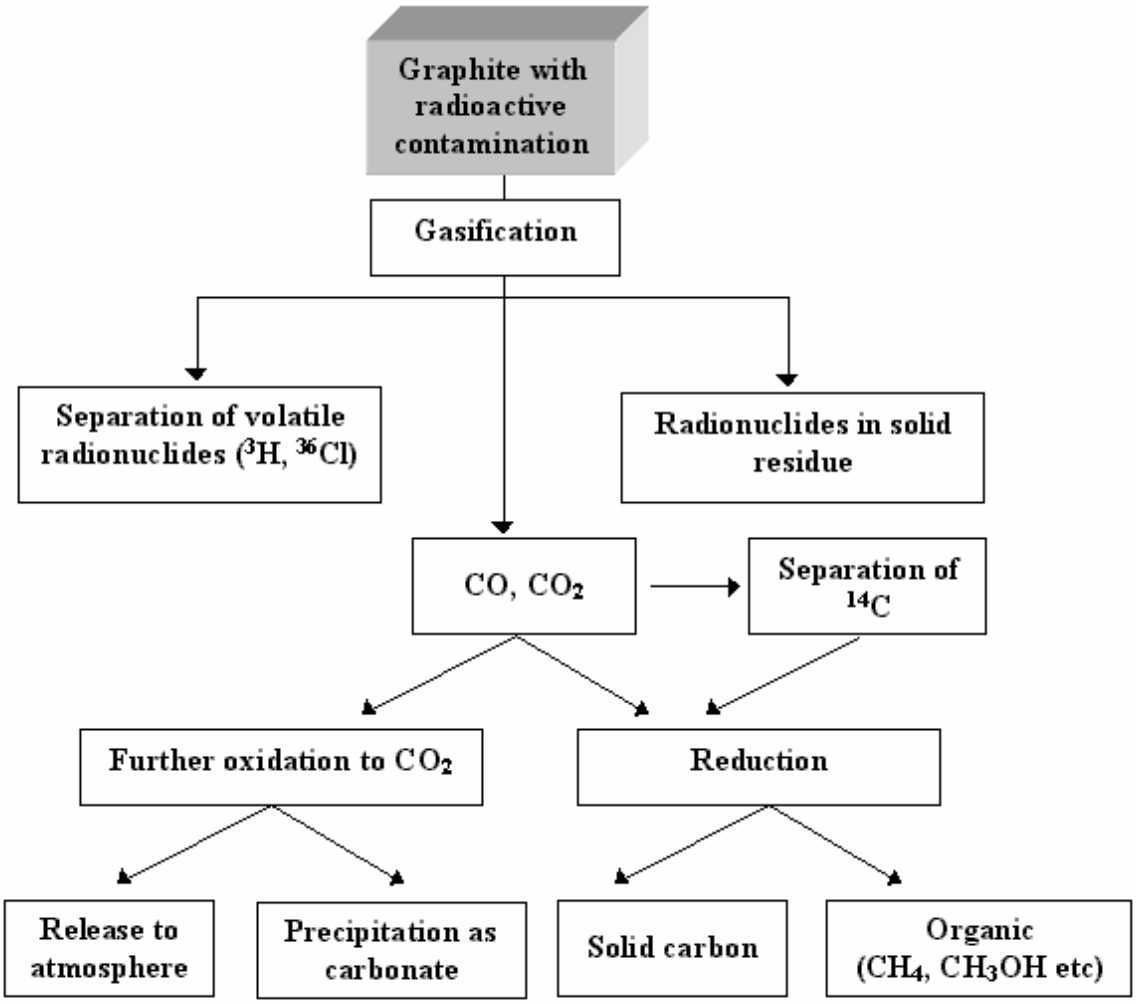

Figure 7. Graphite treatment scheme

4 Experimental part

4.1 Equipment

The following technical equipment was used.

Furnace	combustion furnace C-5500 from Ströhlein Innstruments; tube furnace, adjustable up to 1550°C
Balance	MP-3000, YMC Europe GmbH
CO, CO_2 -analyzer	NGA 2000 MLT analyzer from Fisher-Rosemount, concentration range 0-4000 ppm
Flow controller	mass flow controller 5850E, Brooks fluid: air range: 0 - 70 L/h
γ-spectrometer	High-Purity Germanium Well Detector from EG&G Ortec
Water purification	Elga Elgastat maxima HPLC the specific resistance of purified water is 18.2 mΩ

4.2 Reagents and investigated materials

The following chemicals were used:
NaOH, CuO, HCl, HNO_3
All chemicals were from MERCK, Darmstadt, and of analytical grade. They were used without preliminary treatment.

Investigated materials:

Merlin reactor graphite:	bottom right channel of thermal column II
AVR graphite:	inner reflector

Gases:

Argon:	purity >99.999%, MESSER Grisheim
Oxygen:	purity >99.5%, LINDE
Calibration gas:	mixture CO-1880 vpm, CO_2-2180 vpm, O_2– 0.516 vol%, H_2 – 4 vol%, N_2- rest; MESSER Grisheim

4.3 Performance of experiments

A scheme of the installation for graphite treatment is shown in Figure 9. It consisted of argon flask, a flow controller, an evaporator, an oven with quartz reaction tube, 5 washing bottles and a CO-CO_2 IR-detector. Before the experiment graphite sample was placed in ceramic boat and weighed. Then ceramic boat was pushed slowly into the quartz tube, which was placed in furnace, and heated up to required temperature. The treatment was conducted in inert (argon) and oxidising atmosphere (water steam). The experimental details are listed in Table 6 and Table 7 respectively.
One experiment with the same sample of Merlin graphite was performed with water vapor pressure 70 kPa with temperature increasing (Table 8).

Table 6. Radioactive graphite treatment in argon atmosphere

Sample	Mass, g	T, °C	Time, hours	Flow rate, L/min
Merlin graphite bulk sample	1.3644	866	18	0.12
Merlin graphite powder	0.4023	969	9	0.12
Merlin graphite powder	0.15	1050	15	0.175
Merlin graphite bulk sample	0.9116	1063	13.5	0.12
AVR graphite	0.213	1057	15	0.08

Table 7. Radioactive graphite treatment in water steam atmosphere

Sample	Mass, g	T, °C	Time, hours	P_{H2O}, kPa	Flow rate, L/min
Merlin graphite powder	0.439	1050	9.41	2.3	0.12
Merlin graphite bulk sample	0.446	1050	25.24	2.3	0.145
Merlin graphite powder	0.239	1060	11	7.4	0.66
Merlin graphite powder	0.2262	960	9.42	7.4	0.08
Merlin graphite powder	0.249	960	6.51	7.4	0.66
AVR graphite powder	0.087	1060	15.8	2.3	0.17
AVR graphite powder	0.0726	1070	13.1	31	0.17

Table 8. Oxidation of Merlin graphite powder at increasing temperature

Sample	Mass, g	T, °C	Time, hours	P_{H2O}, kPa	Flow rate, L/min
Merlin graphite powder	0.459	400	5	70	0.145
		600	5	70	0.145
		800	5	70	0.145
		955	5	70	0.145
		1055	5	70	0.145

Argon was flashed through the whole system. The carrier gas was saturated with water vapour by passing through evaporator in the case of experiments with water steam oxidation. Volatile radionuclides were caught in washing bottles. The first washing bottle was filled with 40 ml

0.1 mol/l nitric acid. Tritium as HTO was absorbed in this bottle. After first washing bottle the concentration of CO and CO_2 in gas flow was detected by CO-CO_2-analyzer. Then carrier gas passed through reactor tube with CuO at temperature 550°C in order to oxidise tritium, also presenting as triated molecular hydrogen in the gas mixture, and carbon monoxide to H_2O and CO_2 correspondingly. Oxidised molecular hydrogen were absorbed in the second and third bottles with 0.1 mol/L nitric acid. $^{14}CO_2$ passed the first three bottles and was absorbed in the fourth and fifth washing bottles, which are filled with 40 ml 4 mol/L NaOH. The third and fifth bottles were set to control that all tritium and ^{14}C had been absorbed in the previous washing bottles.
The determination of mass loss of the sample during the time was detected by IR-spectrometer from CO and CO_2 concentration in flow. Before every run the detector was calibrated with a calibration gas with known concentration of CO and CO_2.
After the oven has been heated up to the proper temperature, samples of liquid phase 3 ml in the case of treatment of Merlin graphite and 1.5 ml in the case of AVR graphite have been taken from washing bottles in certain time intervals.
When the experiment was finished, the solutions in the washing bottles were replaced by fresh solutions and graphite was burnt completely in oxygen atmosphere. Then the content of washing bottles was analysed in order to determine the total amount of tritium and ^{14}C in graphite sample.
After complete combustion the ceramic boat was put in a beaker with 30 ml of hot concentrated HCl, heated for 2 hours and left for 24 hours. The liquid was evaporated up to dry residue and dissolved in 5 ml of 2 M HNO_3.
In order to determine the radionuclide transport during treatment procedure reactor tube was divided into several sectors (sectors 1-4 Figure 8) and washed out step by step with concentrated HCl plus 1 mL of HF.

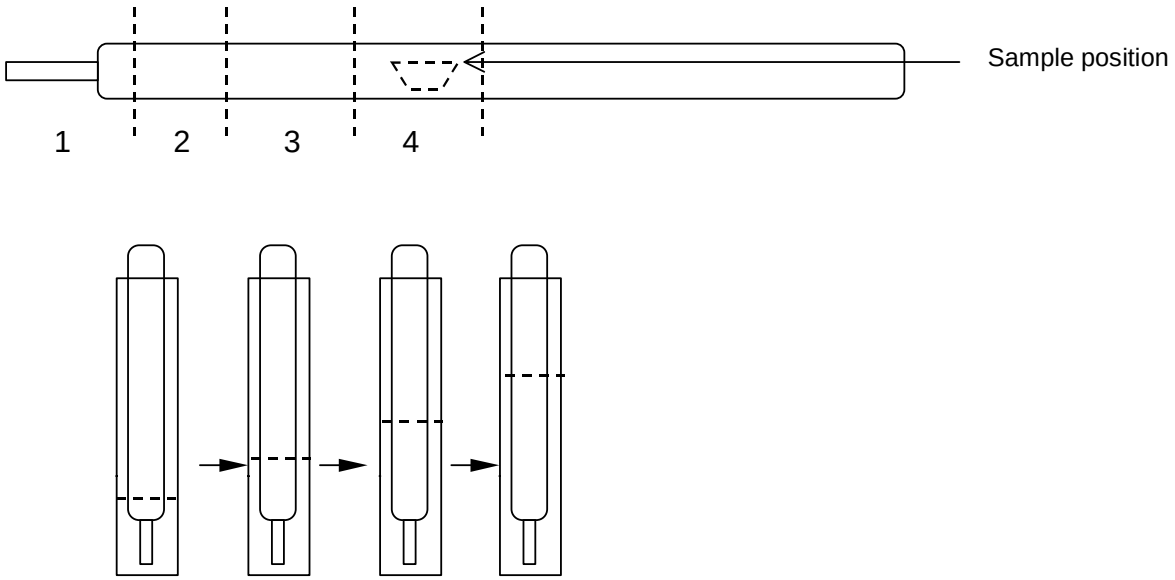

Figure 8. Washing procedure of reactor tube

Then the washing liquid was evaporated up to dry residue and recovered with 5 ml of 2 M HNO_3 (the same procedure as with boat).

Also after the washing procedure the reactor tube and the ceramic boat were analysed by γ-spectrometry in order to ensure that all radioactivity was removed.

Determination of ^{3}H

Tritium was retained in three first bottles with 0.1 HNO_3 solution. In the experiments with Merlin graphite an aliquot of 2 mL was mixed with 18 mL Instant Scint-Gel Plus™ and measured directly by LSC. In the experiments with AVR graphite an aliquot 100 µL was taken from bottles with HNO_3 mixed with 1.9 mL distilled water and 18 mL of Instant Scint-Gel Plus™.

Determination of ^{14}C

An aliquot of 1 mL of solution from fourth and fifth washing bottles was taken, mixed with 1 mL disstilled water and 18 mL of HIONIC FLUOR™ and directly measured with LSC.

Determination of total β,γ-activity

An aliquot of 100 µL from the dissolved residue was diluted with 1.9 mL H_2O and mixed with 18 mL of Instant Scint-Gel Plus™ and then directly measured by LSC.

Determination of γ-activity

An aliquot of 0.5 mL from the solution of dissolved residue was taken, diluted with 9.5 mL of H_2O in plastic 10 mL bottle and measured with γ-spectrometry.

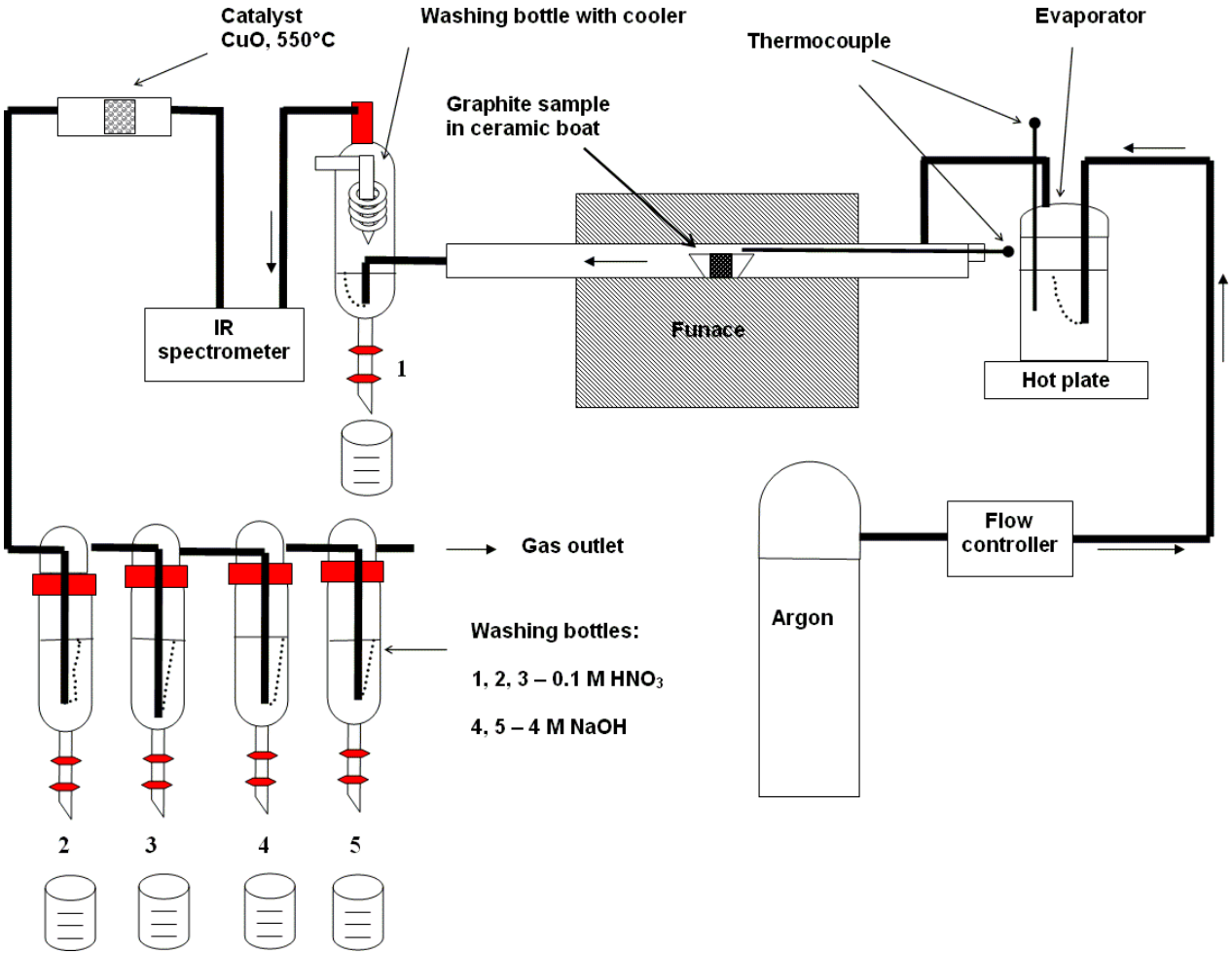

Figure 9. Installation for graphite thermal treatment

5 Results and discussion

In order to study the release of radionuclides during graphite treatment at high temperature, experiments in inert and water steam atmosphere were carried out. The investigations were performed with graphite samples from Merlin reactor and AVR.

5.1.1 Treatment in argon atmosphere

5.1.1.1 Tritium release

The amount of tritium released from Merlin and AVR graphite at different temperatures in inert atmosphere is shown in Figure 10.

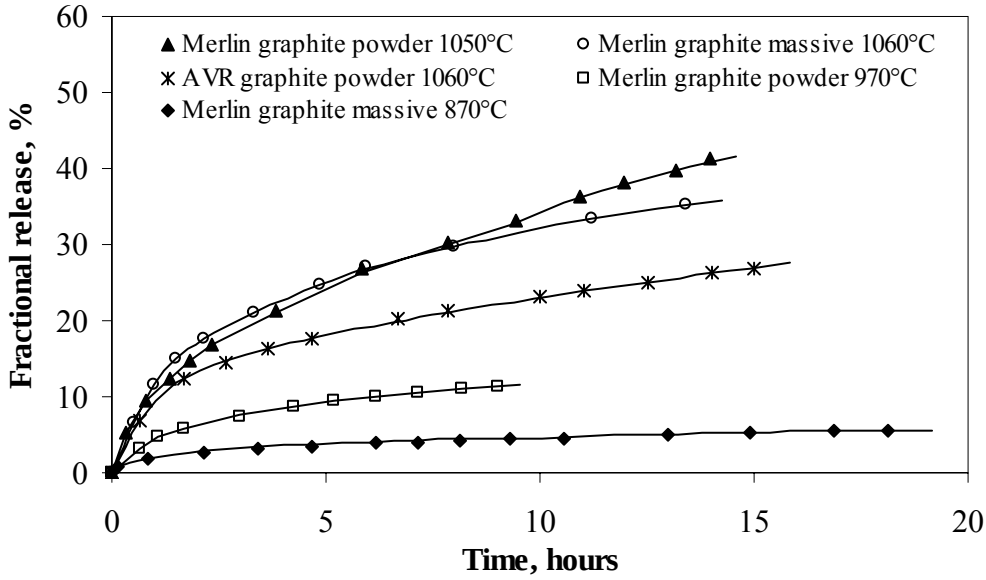

Figure 10. Tritium release in argon atmosphere

In all experiments, two different tritium release stages were observed. In the beginning tritium released faster that corresponds to the region of the release curves with high ascending slope. This can indicate that desorption of ^{3}H from active sites, situated on the surface, occurred. On the second stage the release became moderated with time and had the linear character.

Two samples of Merlin graphite were investigated at the temperature of 1060°C: powder and massive. It can be seen that the amount of released ^{3}H was almost the same for both samples. Therefore it can be considered that tritium release from the graphite sample was not limited by diffusion in pores. The increase of ^{3}H release from powder sample in comparison with massive sample after 9 hours can be explained by oxygen ingress into the system that caused oxidation of graphite sample and increase of released tritium.

The maximum value of released tritium was obtained from Merlin graphite powder. It amounted to 43% after 15 hours. Reduction of the temperature caused a decrease in ^{3}H release. At 970°C the released amount of tritium was about 10 % after a 9-hour treatment.

For AVR graphite the amount of evolved tritium at the same temperature was approximately 27 %. This difference can be explained by different operational conditions for both these

materials. AVR - pebble-bed gas-cooled reactor and the average gas-outlet temperature was about 950°C [13, 39], whereas in Merlin reactor, light water is moderator and coolant. The operational temperature of thermal columns is ambient in this case [40].
It is reported in a number of publications that the mobility of hydrogen molecules in undamaged graphite is rather slow [27, 41, 42]. In AVR the operational temperatures are rather high and some of the defects caused by neutron irradiation can be annealed. The other reason can be referred to the fact that at high temperature conditions of AVR tritium diffuses inside graphite crystal [27, 43].

5.1.1.2 ^{14}C release

^{14}C release is given in Figure 11. The maximum value was obtained for Merlin graphite at 1050°C and amounts to 20 %. The release of radiocarbon is slightly higher in the initial period of time. This possibly represents the elimination of ^{14}C in the composition of oxygen complexes from the graphite surface, which can be easily eliminated by heating. The other possibility can be an interaction of carbon with adsorbed oxygen. A drastic increase of ^{14}C release in this experiment after 9 hours of heating was referred to oxygen ingress as it was mentioned above. One can see that oxidation of graphite increased the radiocarbon release twice despite the mass loss of the sample was not significant (1.36 %).

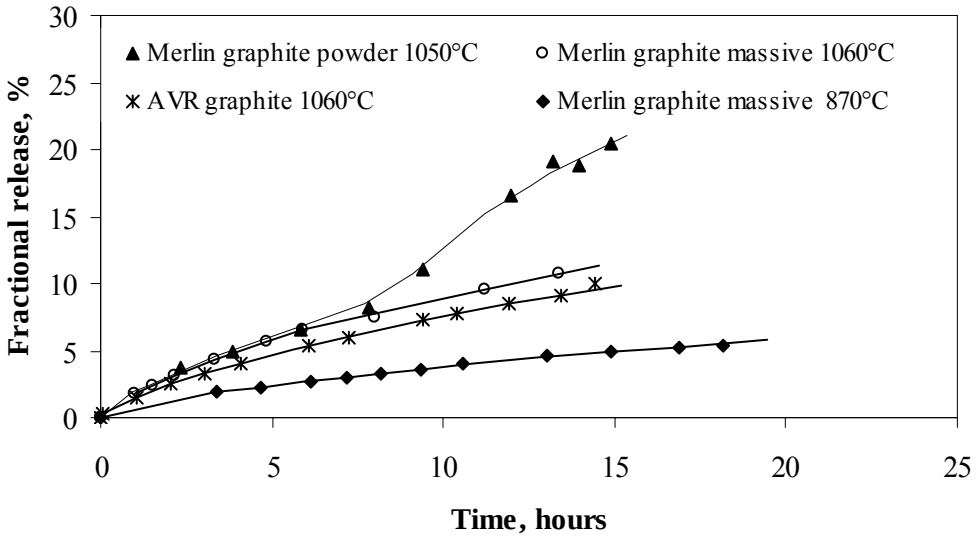

Figure 11. ^{14}C release from AVR and Merlin graphite in argon

The total fractional release of ^{14}C is less than tritium because the location of these radionuclides in graphite matrix is different. That will be discussed later in chapter D.1.3.
It should be noted that during thermal treatment in argon atmosphere small concentration of CO and CO_2 was observed in carrier gas outlet. However, the sample mass loss was negligible and amounted to 0.16-1.36%.

5.1.2 Oxidation with water steam

In order to study the influence of oxidation on the release of tritium and ^{14}C experiments in water vapour were carried out. The saturated water vapour pressure was 2.3 kPa and 7.4 kPa. Additionally one experiment with Merlin graphite was performed in water steam vapour pressure 70 kPa with successive increasing of treatment temperature.

5.1.2.1 Tritium release

^{3}H release during graphite oxidation at stepwise increased temperature is shown in Figure 12. Tritium started to release at 400°C in small amounts (1.3 % after 5 hours). As it can be seen from the release curve slope, the release rate increased with temperature. The whole tritium inventory was removed from graphite sample after 20 hours of thermal treatment. The total mass loss of the sample amounted approximately to 50 %.

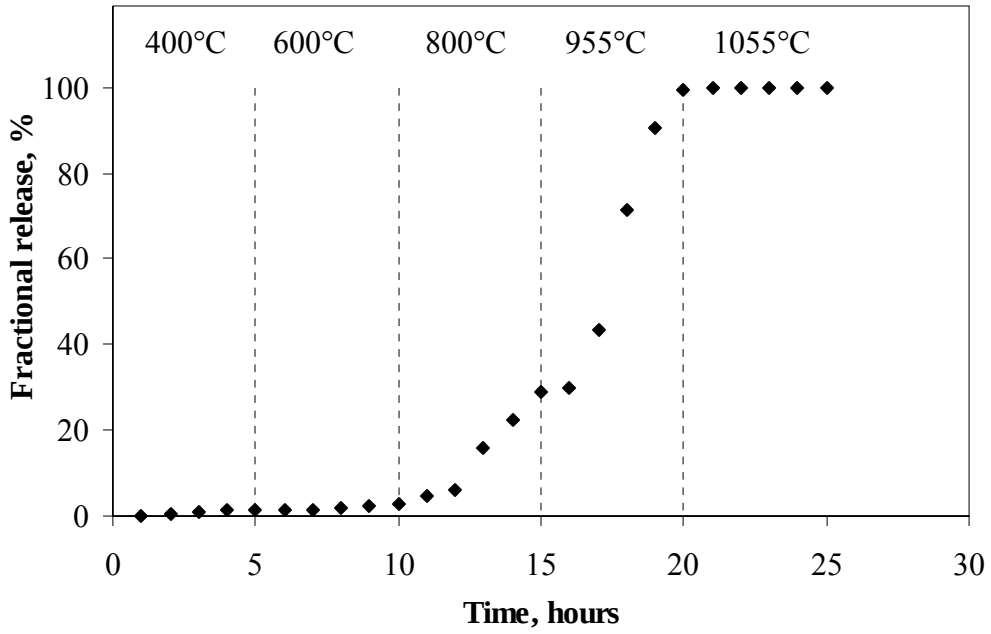

Figure 12. Tritium release with step-by-step temperature increase by oxidation in water steam vapour pressure 70 kPa

^{3}H release from Merlin graphite powder at temperature of 960°C and 1060°C during oxidation with water steam vapour pressure 7.4 kPa is presented in Figure 13 (a). The graphite oxidation leads to increase of the total tritium release in comparison with the experiment in argon atmosphere (see chapter D.1.1 Figure 11).
At 960°C experiments were performed with two different flow rates. The influence of flow rate on ^{3}H release was observed: the increase of argon flux from 80 ml/min to 660 ml/min gives a more than two times increase of released tritium from 30 % to 65 %. The sample mass loss in these experiments was 3.2 and 4 % respectively (Figure 15 b) that is higher in comparison with graphite treatment in argon atmosphere.

At 1060°C, about 90 % of total tritium inventory was removed from Merlin graphite after 8 hours accompanied by a sample mass loss of 32 % (the mass loss of the samples with a time is shown in Figure 15 b in chapter D.1.2.2).
The results of graphite treatment at lower water vapour pressure (2.3 kPa) are shown in Figure 13 b. One can see that the same amount of tritium was released from Merlin graphite at the temperature of 1060°C after 8 hours as in the experiment with water vapour pressure 7.4 kPa (Figure 13 (b)). The corresponding sample mass loss was 22% (Figure 16 b). For AVR graphite fraction of released tritium is less than from Merlin graphite as well as in experiments under inert atmosphere.

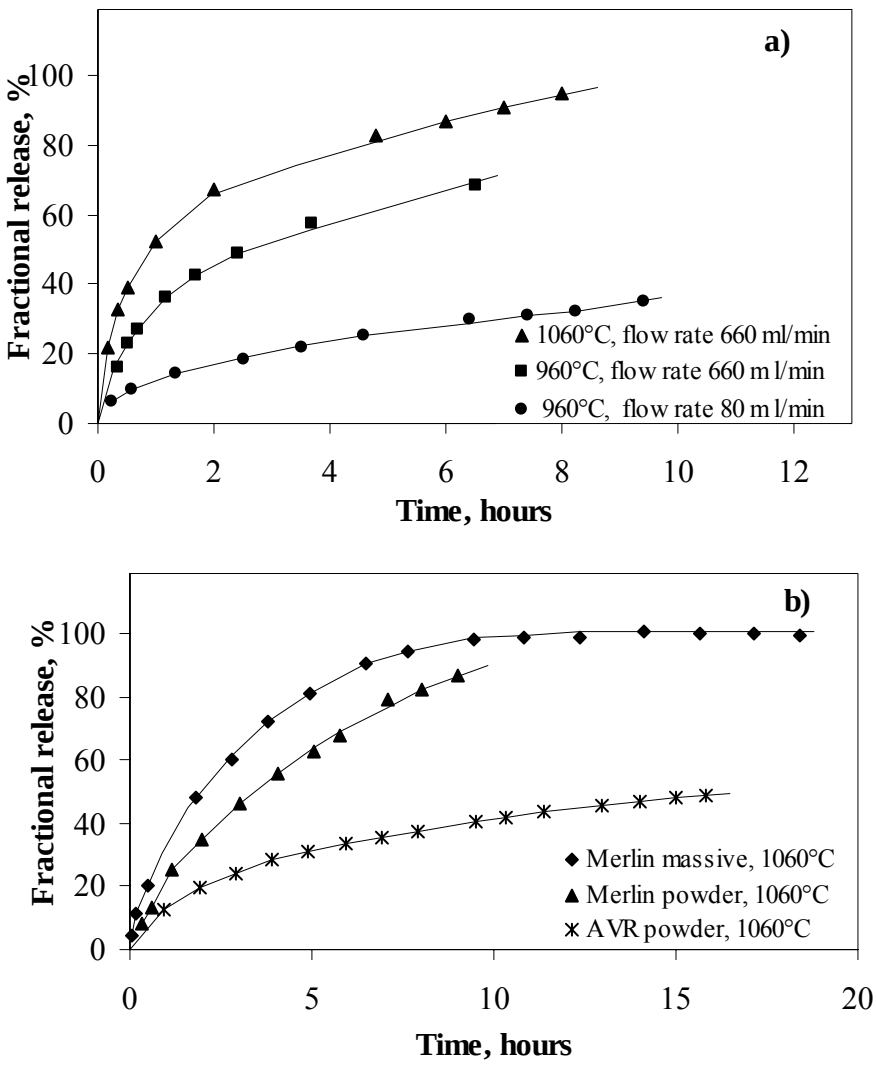

Figure 13. a - tritium release from Merlin graphite powder during oxidation at saturated water vapour pressure 7.4 kPa; b - tritium release from Merlin and AVR graphite at 1060°C and saturated water vapour pressure 2.3 kPa

5.1.2.2 ^{14}C release

The oxidation process influences the ^{14}C release in a similar way as in the case of tritium. As it was shown in the experiments with stepwise increasing of oxidation temperature, ^{14}C release started at 600°C (Figure 14). The quantity of evolved ^{14}C was very small due to negligible reaction rate of graphite and water steam at this temperature. At 800°C a fast increase of radiocarbon release (about 18 % after 1 hour) was observed in the beginning. After that ^{14}C release was rather slow. It can be referred to graphite surface oxidation by adsorbed oxygen. Probably, the ingress of air occurred during cooling the system between experiments, when argon flashing was stopped. Oxygen from the air could be adsorbed chemically on graphite surface and removed trough CO and CO_2 formation after next heating stage.

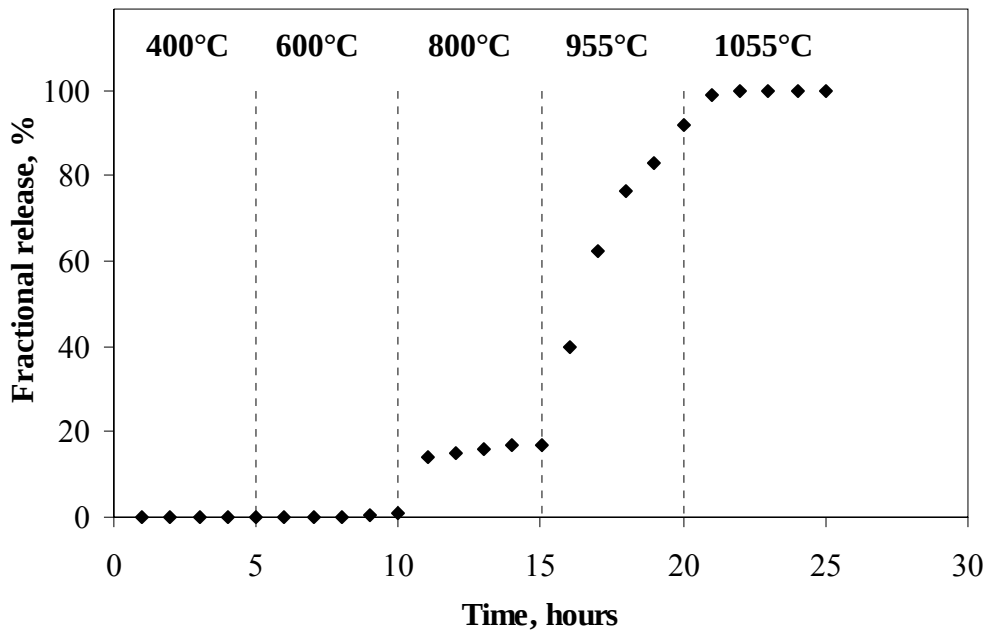

Figure 14. ^{14}C release with step-by-step temperature increase by oxidation in water steam vapour pressure 70 kPa

Based on these results further experiments were performed at temperatures above 900°C because significant ^{14}C release by treatment in water steam was observed under these conditions. ^{14}C release from Merlin and AVR graphite is presented in Figure 15 (a, b).
It can be seen from Figure 15 a Figure 16 a that elimination of radiocarbon increases in comparison with treatment in argon Figure 11. This is connected with oxidation of graphite matrix, leading to release of ^{14}C located in the nodes of graphite lattice.
In order to compare the release of ^{12}C and ^{14}C simultaneously, the mass loss of the sample with time was determined that is presented in Figure 15 b and Figure 16 b. One can see that the loss of 65 % inventory of ^{14}C after 14 hours at 1060°C corresponds to the mass loss of ~ 42 %. As a result we have the ratio about 1.5 for released ^{14}C to oxidized ^{12}C.
At the temperature of 960°C an experiment was performed with two different flow rates. As in the case with tritium, with increasing of flow rate the amount of ^{14}C released also increased from 11 % to 24 % after 7 hours. The mass loss of graphite sample amounted to 2.5 and to 4 %

respectively. This gives the ratio of released isotope's fractions 4.4 and 6, correspondingly. Comparing these results with treatment at a higher temperature (1060°C), after 7 hours it can be concluded that the graphite oxidation at a lower temperature is more effective in order to eliminate ^{14}C without significant burn-off of the total graphite mass.

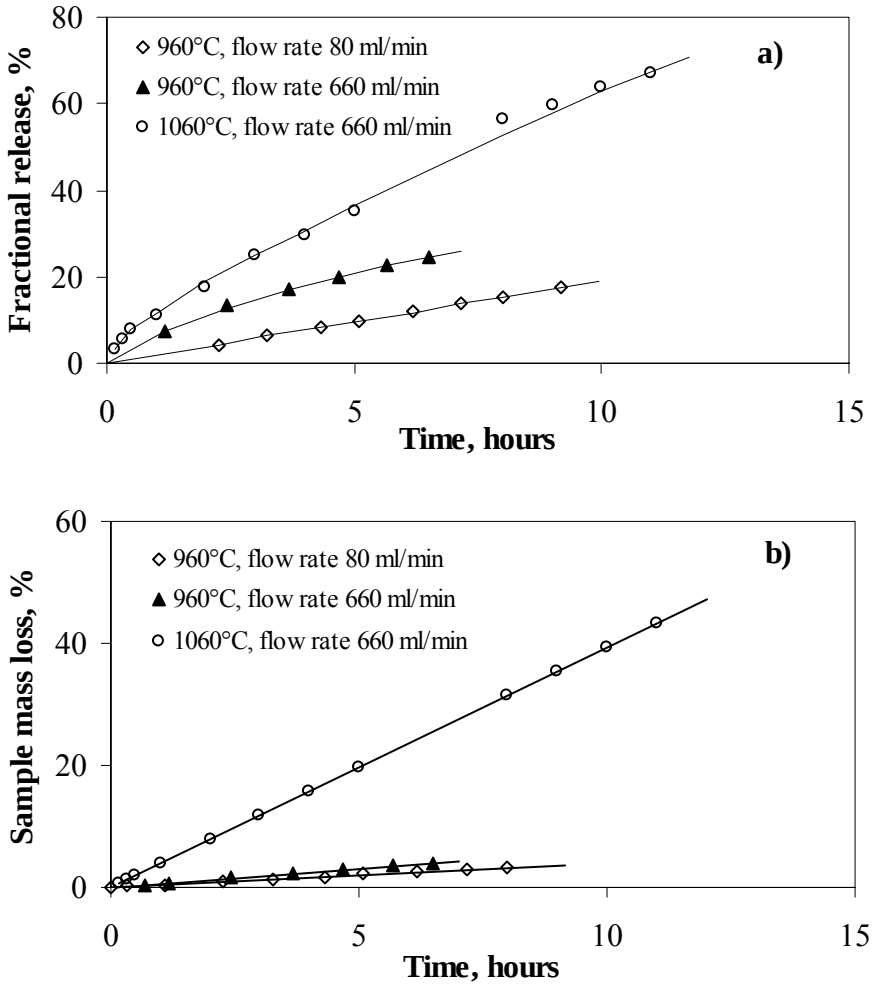

Figure 15. ^{14}C release (a) and mass loss (b) during Merlin graphite oxidation with water steam (water vapour pressure 7.4 kPa)

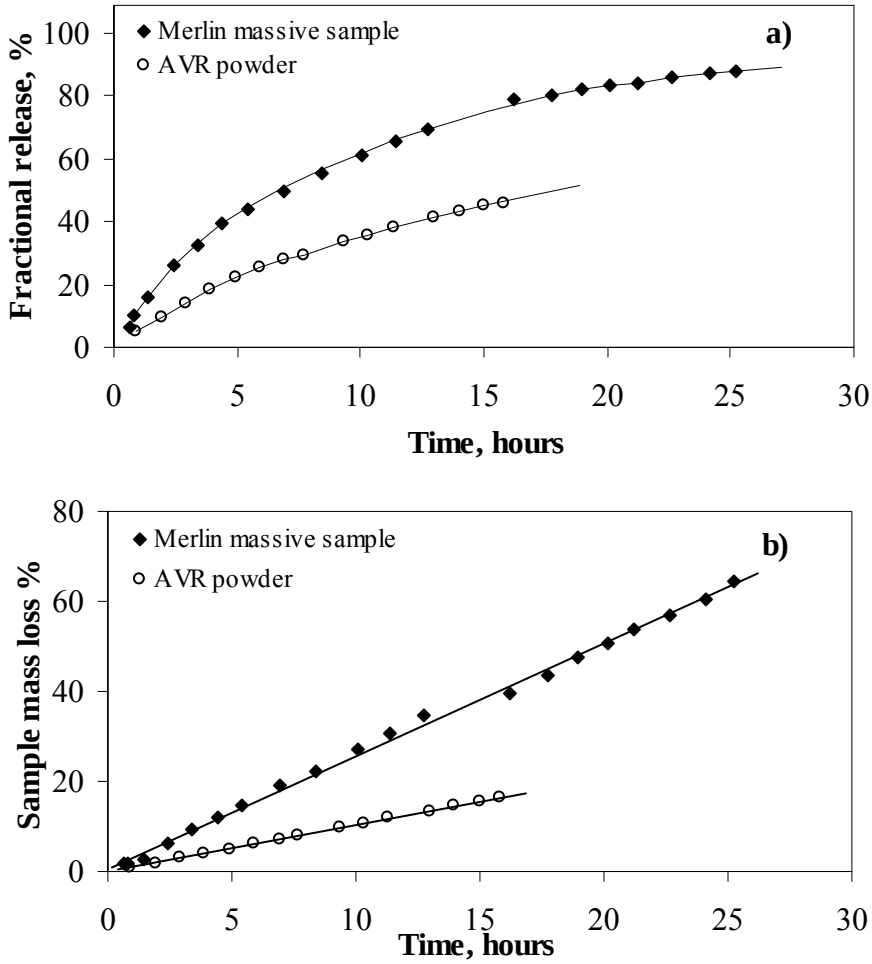

Figure 16. ^{14}C release (a) and mass loss (b) during Merlin and AVR graphite oxidation with water steam (water vapor pressure 2.3 kPa)

5.1.3 Release rates

The kinetics of radionuclide *i* release can be described in the form of release rates R_i. The release rates of radionuclides were determined by following equation:

$$R_i = \frac{x_i(t_j) - x_i(t_{j-1})}{m(t_{j-1}) \cdot (t_j - t_{j-1})} \qquad \text{Eq. (14)}$$

$x_i(t_j)$ - the released amount of component *i* at the moment of time t_j, (mol)

t_j - time at the moment *j*, (hours)

m_{t_j} - mass of the graphite sample at the moment t_j, (g)

The release rate of radioactive components such as ^3H and ^{14}C is certainly much less than oxidation rate of ^{12}C because their content in graphite is very small (10^{-11}mol/g of ^3H and 10^{-10} mol/g of ^{14}C in Merlin graphite). However, the fractional release of tritium and ^{14}C is higher than fraction release of ^{12}C. For example following graph (Figure 17) shows the release

rates and released amount of ^{12}C, ^{14}C and ^{3}H from Merlin graphite (massive sample) during oxidation in water steam at 1060°C and 2.3 kPa water vapour pressure.

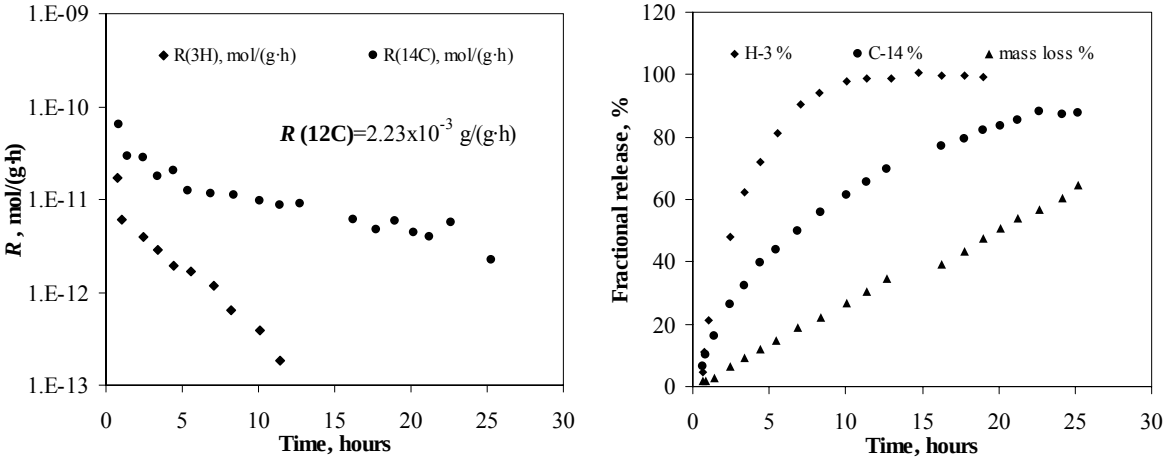

Figure 17. Release rates and released amounts of ^{14}C, ^{12}C and ^{3}H from Merlin graphite oxidised in water steam at 1060°C and water vapour pressure 2.3 kPa.

The release rate of radioactive elements can be compared directly with those of the other elements by normalising with the factor f_i, which is the molar fraction of element *i* in graphite body. Normalised release rate of components was determined as:

$$NR_i = \frac{R_i}{f_i} \qquad \text{Eq. (15)}$$

$$f_i = \frac{\nu_i}{\nu_{^{12}C}} \qquad \text{Eq. (16)}$$

where ν_i - amount of element *i*, (mol)

The ratio of normalised release rate of radionuclide *i* to normalised release rate of matrice component (^{12}C) can be denoted as:

$$K_i = \frac{NR_i}{NR_{^{12}C}} \qquad \text{Eq. (17)}$$

5.1.3.1 Release rates under inert atmosphere

Tritium normalised release rates

The ratios of tritium normalised release rates under inert atmosphere are presented in Figure 18. It can be seen that at all temperatures in inert atmosphere tritium evolved faster than ^{12}C from graphite matrix. The release rate ratio decreased with a time and later became constant. The high rates ratio in the beginning can be referred to desorption of radionuclides form edge planes of graphite and imperfections of graphite structure. The ratio of release rate of ^{3}H to ^{12}C increases with the increase of treatment temperature from 10 at 870°C to ~50 at 1060°C.

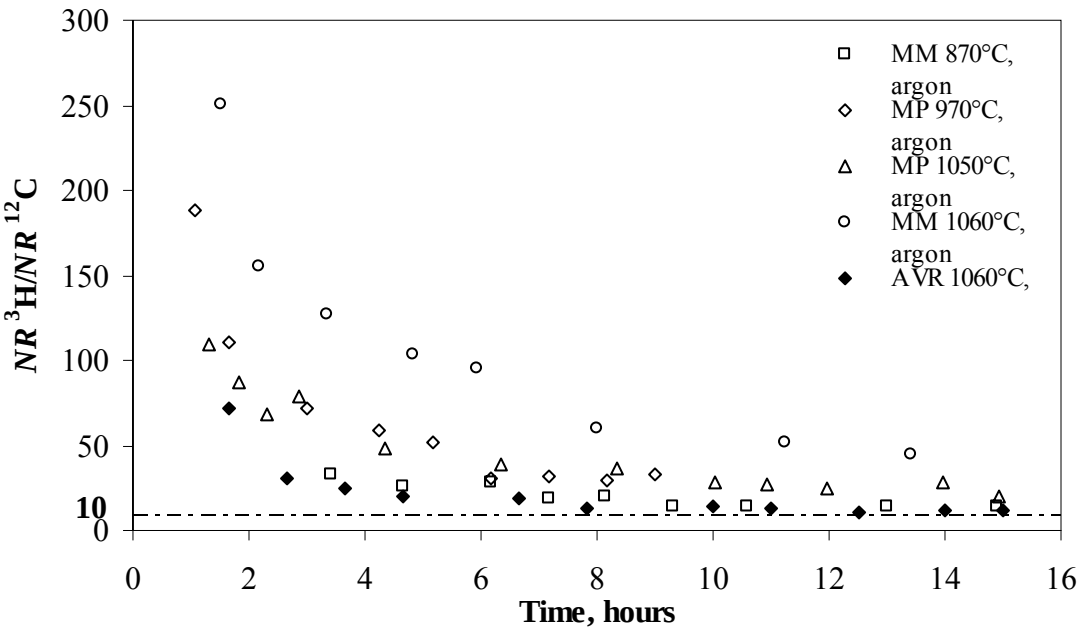

Figure 18. Ratio of normalised release rates of ^{3}H to ^{12}C in inert atmosphere

As it was established [44], hydrogen atoms are trapped at the edges of the graphene sheets and between the graphene layers near the particle surface. Two kinds of trapping sites exist for hydrogen retention [45-47]. One is an interstitial cluster loop edge or solitary dangling bond located in a crystallite with adsorption enthalpy 4.4 eV. The other is a carbon dangling bond located at the edge surface of a crystallite with an enthalpy 2.3 eV [47] (Figure 19). In the case of neutron or ion irradiated graphite the Trap 1 sites dominate hydrogen retention and Trap-2 are important in the case of unirradiated graphite.

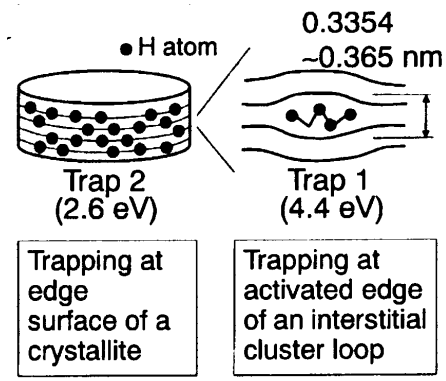

Figure 19. Model of hydrogen trapping sites in a graphite material

Desorption of hydrogen starts at ~300°C and has two maxima around 450°C and 780°C [48]. The first peak is considered due to hydrogen desorbed from defective sites between graphite sheets, and the second one originates from the covalent bonding sites.
The release of tritium from graphite grains is controlled by diffusion process. Tritium atoms desorb from the trapping sites. Then their association reaction takes place at the open pores as

well as on the inner and outer surface of polycrystalline particles, and tritium molecules can diffuse away through open pores to free space.
The mechanism of tritium diffusion in graphite is investigated in details in literature. Numerous studies have been performed on hydrogen diffusion and retention in graphite [27-30, 45, 46, 48].
The most of commercial graphites are not single crystalline materials, but consist of aggregates of polycrystalline particles. The micro structural model of is presented in Figure 20. It is assumed [29] that the tritium atoms captured by carbon atoms diffuse in a crystalline grain along the *a*- and *c*-axis. In addition, tritium atoms can also diffuse along the grain boundaries [49]. Three distinct diffusion channels are indicated in Figure 20 by arrows: 1 – along the *a*-axis in a grain, 2 – along the *c*-axis in a grain and 3 – along the grain boundary. The diffusion through the path 2 does not appear to be plausible because of the large distance carbon network and hence a considerable large activation energy.
The activation energies for respective channels are E_a=100, E_b=240 and E_c=360 kJ/mol [29].

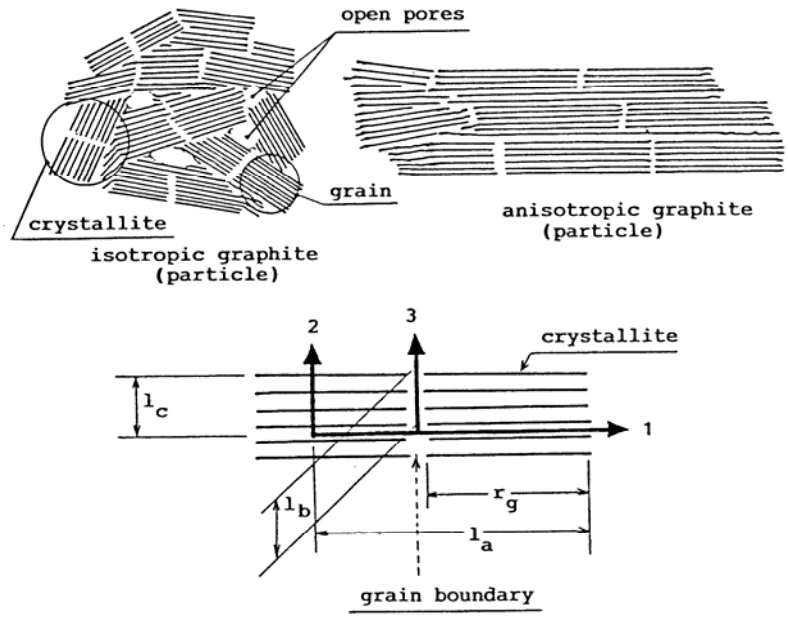

Figure 20. Microstructural models of isotropic and anisotropic graphite

Diffusion coefficients of tritium in graphite

Diffusion coefficients of tritium in graphite can be determined from tritium release curves during isothermal heating of contaminated graphite samples. The fractional release of tritium from graphite *F*(t) can be plotted as a function of the square root of the heating time, *t*(*s*). As it can be seen from Figure 21, tritium release fits well to this function. The diffusion coefficient, *D* (cm^2/s^{-1}) was calculated from the slope of the linear portion of the curve using the following relation which was derived from Fick's law [50]:

$$F(t) = 4\sqrt{\frac{Dt}{\pi}} \cdot \frac{1}{R} \qquad \text{Eq. (18)}$$

for $F(t) \leq 0.3$
R - the recoil range of tritium from $^{6}Li(n,\alpha)^{3}H$ reaction in graphite. The recoil range for graphite was taken from literature and amounted to 32 μm [50, 51]. Results of the calculations are presented in Table 9.

Table 9. Diffusion coefficients of tritium in Merlin and AVR graphite

Type of graphite	Temperature, °C	Diffusion coefficient D, cm^2/s^{-1}
Merlin	870	5.70E-14
Merlin	970	7.40E-13
Merlin	1060	6.19E-12
AVR	1060	1.70E-12

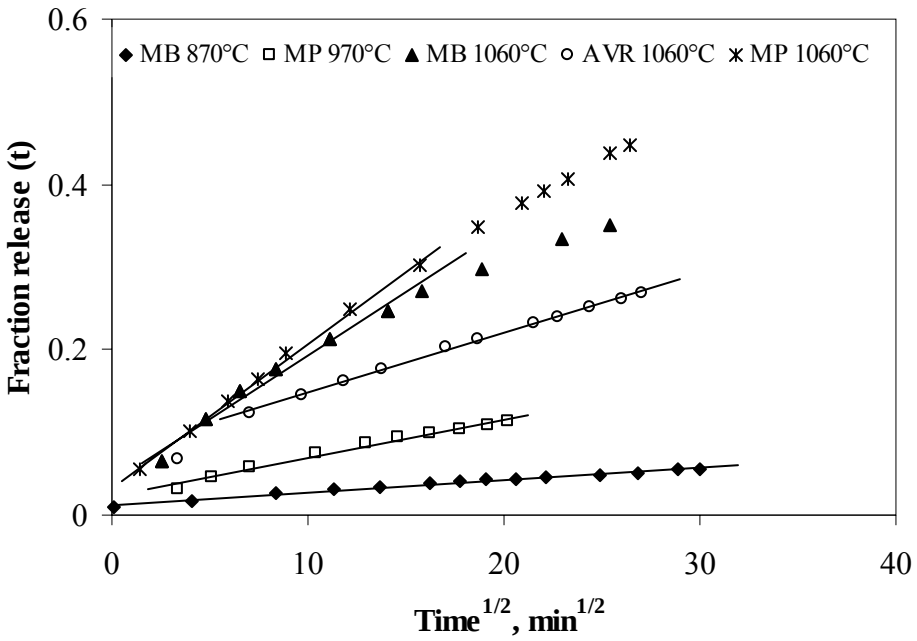

Figure 21. Tritium release vs. square root of the treatment time

Figure 22 shows an Arrhenius plot of logarithms diffusion coefficients for Merlin graphite vs. 1/T (°K). From the slope activation energy was calculated as 312 kJ/mol and the pre-exponential factor calculated was 10.7 cm^2/s.
Pre-exponential factor and activation energy are different for different types of graphite due to classification of the diffusion paths [29]. The diffusion of tritium in highly oriented graphite or highly anisotropic graphite will be slower than in isotropic one, because the tritium atoms hardly penetrate the layer plane. As it was shown by Saeki [30] the activation energy of diffusion process in graphite samples with high value of anisotropy factor was in the range of 250-260 kJ/mol, whereas the activation energy for isotropic pyrographite amounted to 105 kJ/mol. In the case of laminar graphite [51], with a considerably large parameter l_a the activation energy is 412 kJ/mol for diffusion along grain boundaries. The values of pre-

exponential factor and activation energy obtained for Merlin graphite in present work are typical for nuclear graphite with high anisotropy factor.

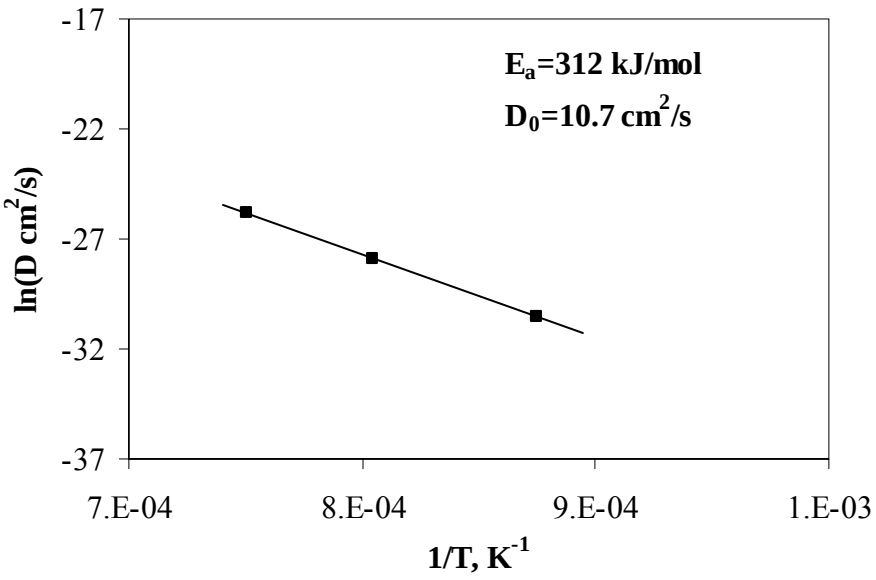

Figure 22. Arrhenius plot for tritium diffusion in Merlin graphite

<u>^{14}C normalised release rates</u>

The ratio of carbon isotopes release rate ($K_{14C/12C}$) was lower than in the case with tritium (chapter D.1.3.1, Figure 18). The highest *K* value was observed for Merlin graphite by treatment at 870°C in argon. As it can be seen from the Figure 23, *K* value was close for Merlin graphite treatment at 1060°C and 870°C. Higher release rate of ^{14}C in comparison to ^{12}C means that this radionuclide is not distributed homogeneously in graphite lattice. Otherwise it would be released with the same rate as ^{12}C. Therefore it can be supposed that graphite surface near grain boundaries is enriched with ^{14}C.

Information about ^{14}C localisation in graphite was not found in literature. It is known that ^{14}C is an activation product originating mainly from nitrogen impurities in graphite matrix or from nitrogen adsorbed on the surface from gas cooler [16]. The contribution of ^{13}C and ^{17}O are of less importance.

One possibility of ^{14}C position in graphite crystal is adsorption on the edge planes of graphite surface. Oxygen functional groups on carbon surfaces decompose to carbon oxides upon heating in an inert atmosphere [52]. The complexes yielding CO_2 were shown to decompose typically over a range of temperatures starting at 200°C and exhibiting desorption maximum at 300°C and 600°C [53]. Carboxylic acids have been proposed to be predominantly responsible for the low- temperature peak. The high-temperature CO_2 evolution has been attributed to carboxylic anhydrides. Similarly, the CO-yielding groups have CO evolution maximum at 900 and 1100 K. The total desorbed quantity of CO and CO_2 amounted to 19 µmol/g for graphitized carbon fibres with specific surface area 6 m^2/g. This corresponds to 0.023 % of mass loss. In present experiments mass loss varied in the range from 0.16 to 1.6 %. Thus this carbon can not be referred only to desorption of functional groups but also to slow oxidation

caused by presence of oxygen traces in the inert carrier gas. Moreover, desorption would take place in the first period of time, whereas we have observed constant release of ^{14}C from the sample during all heating procedure.

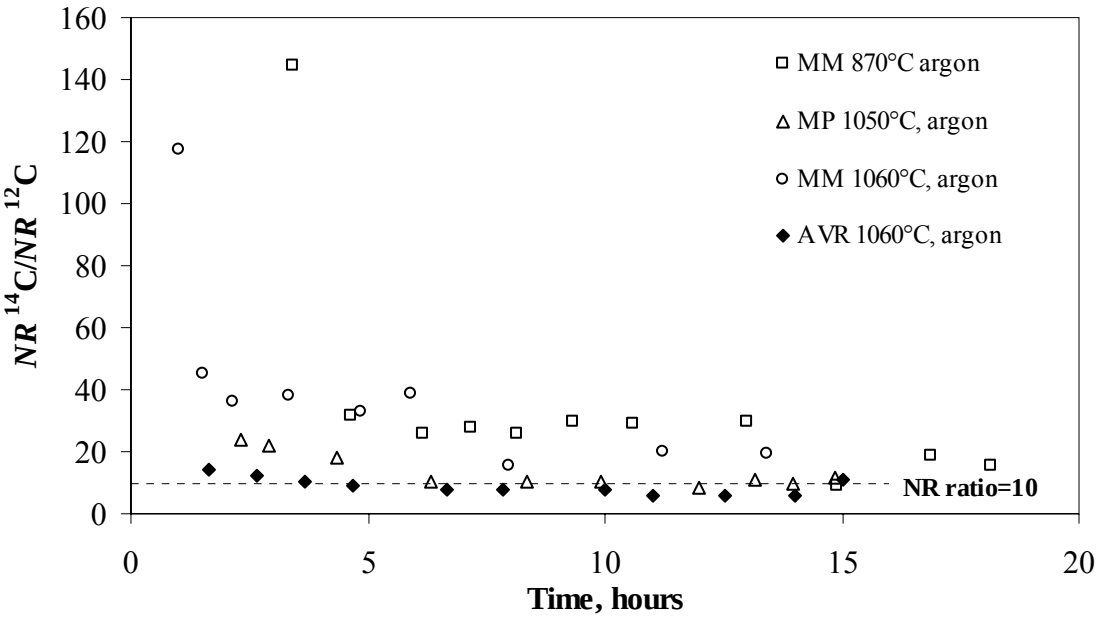

Figure 23. Ratio of normalised release rates of ^{14}C to ^{12}C in inert atmosphere

The other possibility of radiocarbon arrangement in graphite is intercalation between graphite layers or embedding in graphite lattice under neutron irradiation [54]. ^{13}C also can be a source of uniformly distributed in graphite matrix ^{14}C. Being in composition of graphite lattice, ^{14}C can be removed only by oxidation because carbon diffusion in the basal plane is significant only above 2200°C [20].

A carbon atom displacement caused by neutron or ion irradiation results in crystallite dimensional changes [11]. Two types of damage centres are known – vacancies and interstitials. Interstitials cause crystallite growth perpendicular to the layer planes (c-axis direction) and coalescence of vacancies causes shrinkage parallel to the layer plane (a-axis direction). During thermal treatment annealing of the lattice defects occurs. Interstitials start to migrate to the edge surface or to reintegrate with vacancies [11, 55, 56]. If ^{14}C is in the composition of interstitials it can be supposed that during heating in inert atmosphere diffusion of ^{14}C from graphite can be attributed to diffusion of interstitials from interlayer space to the edges of graphite planes with their following desorption. But, as it was already mentioned above, the presence of constant concentration of CO and CO_2 of few ppm in carrier gas flow supposes the presence of oxygen in the system. Therefore the conditions were not absolutely „oxygen free“ and release of ^{14}C caused by oxidation can not be excluded.

5.1.3.2 Release rates under oxidising conditions

Normalised release rates were calculated for oxidation of Merlin graphite with water steam (water vapour pressure 7.4 kPa and 2.3 kPa) at temperatures of 1060°C and 960°C. The release rates ratios of ^{3}H and ^{14}C to ^{12}C are presented in Figure 24 and Figure 25.

It can be seen from Figure 24 that at 960°C velocity of carrier gas effects on the ratio of release rate of tritium and ^{12}C. At lower argon velocity (80 ml/min) K_{3H} was about 10. At higher argon flow velocity (660 ml/min) the ratio of release rates of ^{3}H to ^{12}C increased up to 23.
In the case of ^{14}C it can be seen from Figure 25 that the release rate ratio of ^{14}C to ^{12}C did not depend on the gas velocity and amounted to ~7.
At 960°C the reaction with water steam is closer to the regime of the first reaction zone (see B.1.2) [2]. The reaction rate in this temperature zone is low and is determined by the intrinsic reactivity of the graphite. Different part of the graphite structure may react at different rate: edge atoms being more reactive than basal plane atoms.
The reaction rate of bulk graphite with water steam increased with the temperature up to 1060°C. The ratio of release rates for both radionuclides to ^{12}C release was decreased in comparison with 960°C. After the initial period of time release rate of ^{14}C approached almost the same value as the rate of matrix oxidation. The influence of water vapour pressure on the release rate of radionuclides and matrix oxidation can be observed by comparing the results of graphite treatment at 2.3 kPa and 7.4 kPa saturated water vapour pressure at the temperature of 1060°C. At 7.4 kPa normalised release rates were higher, but the ratio of normalised release rate of tritium to graphite matrix oxidation rate was lower. For ^{14}C this value did not change in comparison with experiments at 2.3 kPa saturated water vapour pressure.

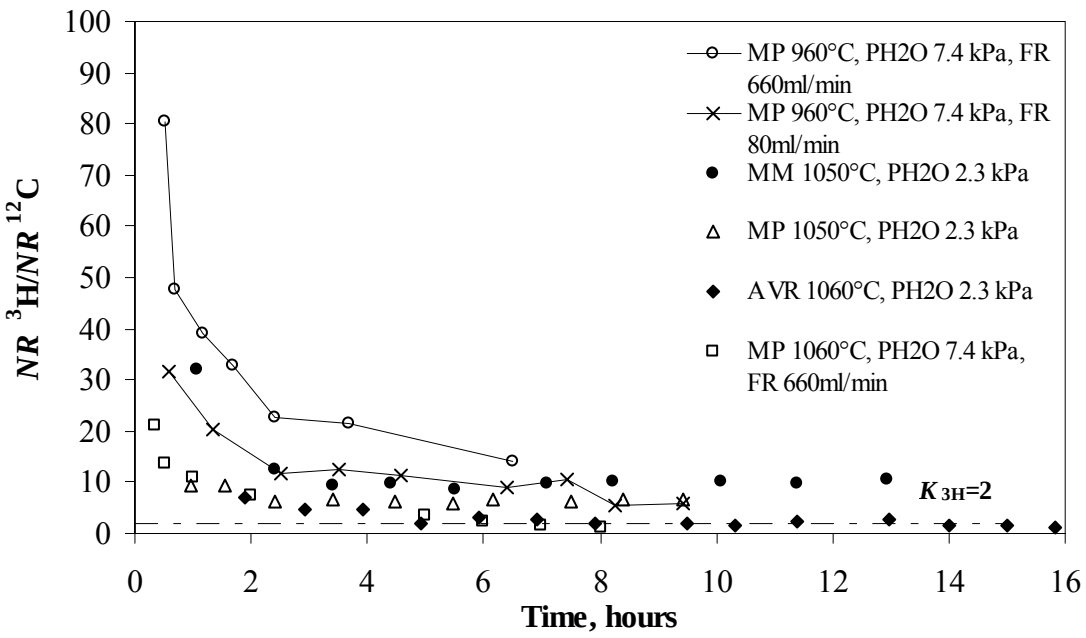

Figure 24. Ratio of normalised release rates of ^{3}H to ^{12}C in oxidising atmosphere

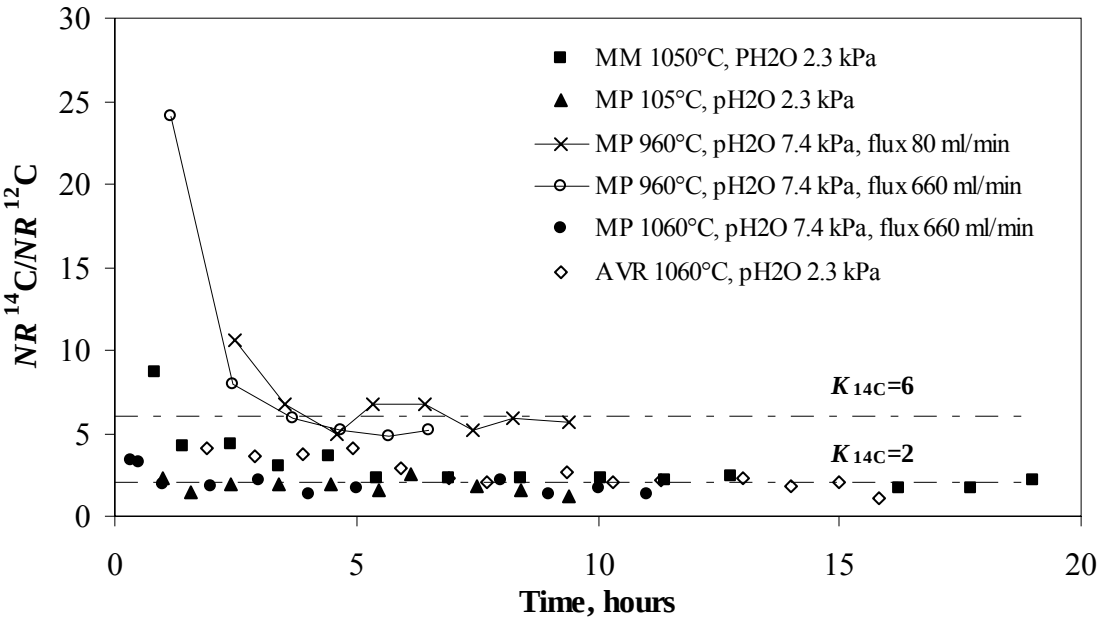

Figure 25. Ratio of normalised release rates of ^{14}C to ^{12}C in oxidising atmosphere

The results obtained for AVR graphite after treatment in water steam differ from those obtained for Merlin graphite. It is typical for AVR graphite that ^{14}C and ^{3}H released with the same rate during oxidation. It can be explained from the fact that tritium in AVR reflector graphite diffuse inside graphite crystal at high temperatures of reactor operation and can be blocked by carbon atoms displaced from the lattice under neutron irradiation into interplanar space. Apparently, during oxidation of graphite release of these trapped tritium atoms occurs.

5.1.3.3 Comparison of treatment regimes

The main parameter determining the efficiency of contaminated graphite treatment without its complete combustion is ratio of fractional release of radionuclides to mass loss of graphite. According to the difference in the release rate ratios of radionuclides depending on treatment conditions, the results on ^{14}C and tritium release are summarised and compared in Figure 26 and Figure 27.

In the case of ^{14}C it can be seen that all the release curves can be generally divided into two groups. The separation, shown by dashed line, differs by ratio of fractional release of radioactive component to the mass loss of ^{12}C. For example, during heating of Merlin graphite in argon at 1060°C, the mass loss amounted to 0.4 % and ^{14}C release about 11 % of its total content, whereas treatment in water steam at 1060°C gives the release value of ^{14}C 11% accompanied by sample weight loss of 6%.

For the group I relatively high ^{14}C release at a small mass loss of the sample is typical. Experiments in argon atmosphere and at low temperature oxidation in water steam belong to this region. The ratio of release rates of isotopes is higher than 5. Oxidation experiments at high temperatures are referred to the group II. Here graphite oxidation rate is rather high and mass loss in comparison with radioactive carbon release is significant. The release ratio of carbon isotopes is about 2.

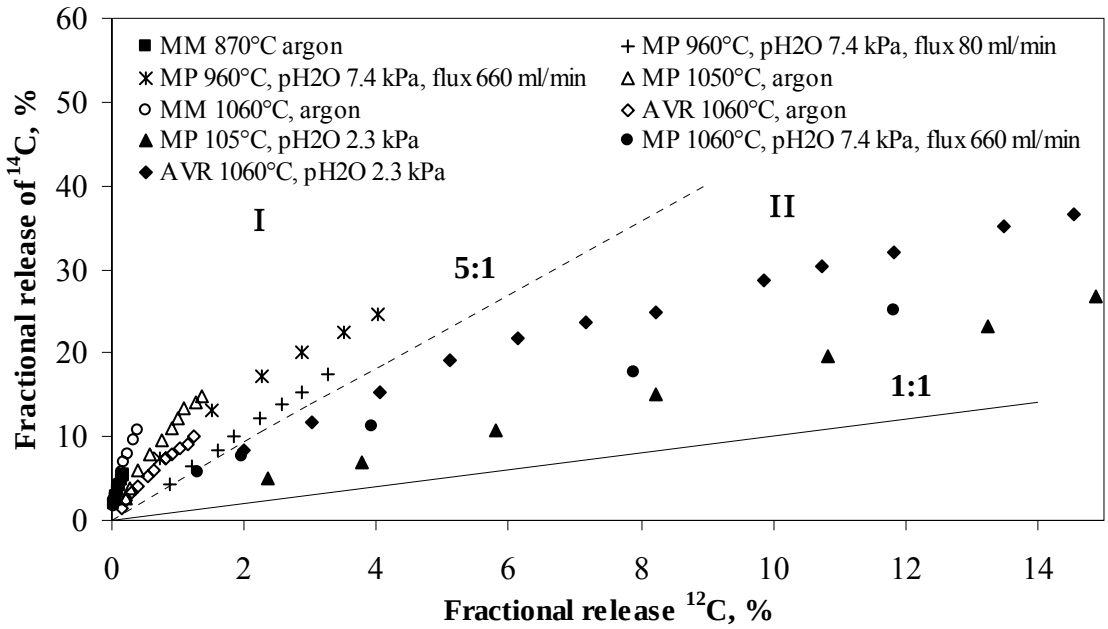

Figure 26. ^{14}C release vs. fractional release of ^{12}C during treatment in different conditions (MM – Merlin graphite massive sample, MP – Merlin graphite powder)

From the Figure 26 region I it can be assumed that ^{14}C release was not caused by diffusion of interstitials from interplanar space because in this case the ^{14}C release on temperature dependence would be clearly seen. Apparently, the graphite grain boundaries are enriched with ^{14}C and its concentration decreases with depth inside graphite grains that can be observed by oxidation of graphite at low temperatures or by small concentrations of oxidant.
A suitable method for ^{14}C release from contaminated graphite is slow selective oxidation of graphite edge planes in order to remove „contaminated“ zone.
In contrast to ^{14}C, tritium fraction release curves in argon atmosphere (region I Figure 27) show significant difference in amount of ^{3}H released at different temperatures by the same mass loss. The experiments in steam at high temperatures lie in the region II below the dashed line 20:1. In this region tritium fractional release is still rather high in comparison with sample mass loss (line 1:1).
It can be considered for tritium that treatment at high temperatures in inert atmosphere is sufficient to release this radionuclide from graphite.

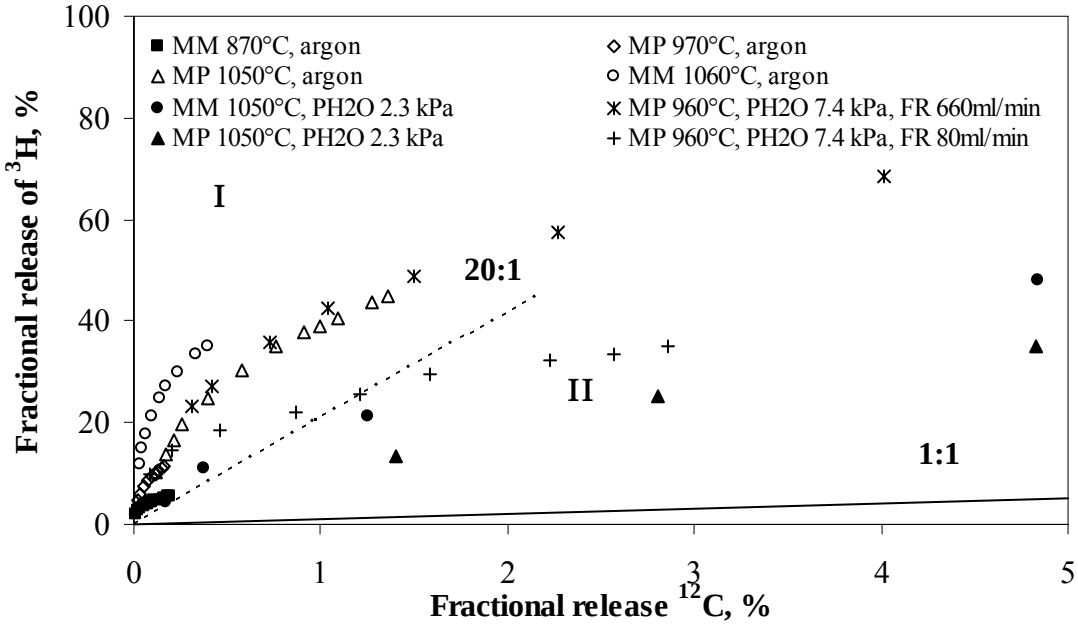

Figure 27. ^{3}H release vs. fractional release of ^{12}C during treatment in different conditions (MM – Merlin graphite massive sample, MP – Merlin graphite powder)

5.1.4 Migration of other radionuclides during graphite thermal treatment

The measured γ-activity of Merlin and AVR graphite correlates with previously data reported [57, 58] (Table 25, Table 26).
In the case of Merlin graphite inventory of the main contaminants such as ^{60}Co, $^{154,155}Eu$ and ^{133}Ba was not very high (Table 26 in appendix).
Analysis of residue remained in reaction boat after complete combustion of graphite sample revealed that virtually all radionuclides stayed in ceramic boat and could be recovered by rinsing in concentrated HCl (Table 10).

Table 10. Results of γ- and total γ, β-activity measurements of Merlin graphite samples

Radionuclide	Average activity Bq/g	960°C p_{H2O} 7.4kPa Bq/g	1060°C p_{H2O} 7.4kPa Bq/g	1060°C argon Bq/g
Eu-152	640	689	742.6	624
Cs-137	0.18	–	–	–
Co-60	536	553	581	389
Total β–γ activity	1355	1258	1312	1419

Average activity was determined in independent experiments by complete combustion of graphite samples in oxygen.
In AVR graphite ^{133}Ba, $^{154, 155}Eu$, $^{134, 137}Cs$ and ^{60}Co are present in larger amounts than in Merlin graphite. After experiments in argon atmosphere for 15 hours at 1060°C, the analysis of reactor tube showed no radionuclide contamination. After post-experimental graphite burning,

^{133}Ba, $^{154, 155}$Eu and ^{60}Co were found almost completely in leachate from ceramic boat. As it was expected from literature data [25], these radionuclides were not volatilised at this temperature and remained in the combustion chamber.
The radionuclide inventory measured in the washing liquid and in boat is listed in Table 11. The total content of every radionuclide was calculated as average from analysis of AVR graphite samples (Table 25 in appendix). Therefore scattering between total amount of radionuclide and its recovery can be attributed to inhomogeneity of radionuclide distribution in graphite.
The behaviour of Cs was less evident. About 30% of from total content was found in the reaction boat. The rest of Cs was considered to diffuse from graphite and later volatilised because of high experimental temperature of 1060°C. It is known that at this temperature Cs can be transported to the gas phase due to volatilisation [12, 25]. However Cs was not detected in the reaction tube rinse and in the washing bottles.

Table 11. Radionuclide distribution after treatment of AVR graphite in argon atmosphere

Radionuclide	Total content	Rinse from reaction boat	Reaction boat
	Activity, Bq		
Ba-133	304±46	233±35	9±1
Eu-154	124±19	100±15	2
Eu-155	33±5	30±5	–
Cs-134	36±5	–	11±2
Cs-137	607±91	5.9±1	200±30
Co-60	2604±390	2500±375	102±15

During steam oxidation of AVR graphite (water vapour 31 kPa) at 1060°C, the contamination of reaction tube was not observed also. The results of γ-analysis of residue and reaction boat are presented in Table 12. It can be seen that the main radionuclide inventory was detected in reaction boat.
This can be effectively used for graphite cleaning from these contaminants.

Table 12. Radionuclides distribution after treatment of AVR graphite in water steam (water vapour pressure 31 kPa)

Radionuclide	Total content	Rinse from reaction boat	Reaction boat
	Activity, Bq		
Ba-133	103±16	18±3	54±8
Eu-154	42±6	9±1	15±2
Eu-155	12±2	5±1	–
Cs-134	12±2	–	10±1
Cs-137	207±31	–	165±25
Co-60	1249±187	15±2	1450±218

6 Summary and outlook

The objective of present work was devoted to the treatment of contaminated graphite with respect to waste management. The main problem associated with direct disposal of contaminated graphite is its large volume. Reprocessing of the graphite, based on the graphite gasification, offers the opportunity to separate the majority of the short-lived isotopes from graphite, which could be further reused. The existing reprocessing scheme allows to separate non-volatile and volatile radionuclides by chemical methods, giving at the end the mixture ^{14}C and ^{12}C. The development of simplified method for graphite purification from ^{14}C would reduce the waste volume and, therefore, diminish the problem of reactor graphite disposal.
In the present work the release of tritium and ^{14}C during thermal treatment of contaminated graphite from Merlin thermal column and AVR reflector was investigated. The experiments were performed in flow of argon and water steam at the temperature range of 870-1060°C. Comparison of release rate ratios of volatilised radionuclides ^{14}C and ^{3}H with release of ^{12}C showed that under all experimental conditions tritium and ^{14}C were released faster than graphite sample was oxidised.
For tritium the maximum value of release rate ratio was obtained in experiments with argon atmosphere and increased with temperature. Tritium originates from activation of lithium impurities, which are present in graphite. It is located on graphite edge planes or between basal sheets. At elevated temperatures tritium started to diffuse from graphite crystals and can be released to gas phase. Diffusion coefficients for Merlin graphite samples at the temperatures 870, 970 and 1060°C were determined. Activation energy of diffusion process and pre-exponential factor were estimated from Arrhenius plot. For Merlin graphite absolute diffusion coefficient can be presented by equation:
$D = 10.7 \cdot \exp(-312\ \text{kJ/ mol} / RT)\ \text{cm}^2/\text{s}$
The performed experiments allow to consider that tritium can be release without significant volatilisation of graphite by oxidation. Diffusion of tritium in different graphite types depends on the conditions of its operation. Graphite irradiated at higher temperatures (AVR graphite) requires longer time to remove tritium.
For ^{14}C the maximum fractional release ratio (^{14}C to ^{12}C) was observed for lower temperatures in experiments with water steam as well as in experiments with argon. Difference in release rates of ^{14}C and ^{12}C allows to assume that ^{14}C is not distributed uniformly in graphite lattice. Otherwise the normalised release rate of ^{14}C and ^{12}C would be the same. As it is known, ^{14}C mainly formed by an (n,p) reaction of nitrogen impurities and from nitrogen impurities adsorbed from cooling gas, is embedded in graphite lattice under irradiation condition. The results of experiments performed indicate that ^{14}C locates mainly near grain boundary surface and its concentration profile decreases with depth. This part of ^{14}C can be released from graphite using low temperature oxidative treatment without significant mass loss.
The behaviour of ^{60}Co, $^{154,155}Eu$, $^{134,137}Cs$ and ^{133}Ba, which are present in contaminated graphite, was also investigated. It was shown that during treatment in inert and oxidising atmosphere these radionuclides, beside Cs, remain mainly in the reaction ceramic boat. During heating at high temperatures Cs can diffuse from graphite sample and later be volatilised into the gas phase.
Separated from the main graphite mass tritium, ^{14}C, and other radionuclides can be collected in concentrated form and handled separately. ^{14}C and ^{3}H could be later reused for commercial

purpose (for example as tracers). ^{14}C also can be converted to carbonates or carbon for disposal with a smaller volume than the original graphite.
This work showed the possibility to deplete the ^{14}C inventory in nuclear graphite by thermal treatment. The separation of radioactive carbon allows to reduce significantly the problem of radioactive waste volume. However, further investigations are necessary before the process can be developed to the pilot scale.

7 References

[1] N.R. Laine, F.J. Vastola, P.L. Walker, The importance of active surface area in the carbon oxygen reaction, *Journal of Physical Chemistry,* **67**, 2030, 1963.

[2] W. Delle, K. Koizlik, H. Nickel, Graphitische Werkstoffe für den Einsatz in Kernreaktoren. Teil 2: Polykristalliner Graphit und Brennelementmatrix, Karl Thiemig AG, München, 1983.

[3] K. Hedden, E. Wicke, About some influences on the reactivity of carbon, 249, Third Biennial Carbon Conference, 1957.

[4] K. Hedden, A. Löwe, Über die Vergasung von Reaktorgraphit mit Kohlendioxid und Wasserdampf, *Carbon,* **5**, 339, 1967.

[5] P.L. Walker, Chemistry and physics of carbon, Vol. 1, 1965.

[6] L. Xiaowei, R. Jean-Charles, Y. Suyuan, Effect of temperature on graphite oxidation behavior, *Nuclear Engineering and Design,* **227**, 273, 2004.

[7] R. Moormann, H.K. Hinssen, K. Kühn, Oxidation behavoir of an HTR fuel element matrix graphite in oxygen compared to a standard nuclear graphite, *Nuclear Engineering and Design,* **227**, 281, 2004.

[8] W. Katscher, R. Moorman, H.K. Hinssen, B. Stauch, Versuche zur Graphitkorrosion in Luft bei Temperaturen unterhalb 873 K, Vorschlag zur Modifizierung des Verbrennungs-Head-Ends für HTR-Brennelemente, Berichte der KFA Jülich, KFA-ISF-IB-2/82, 1982.

[9] G. Haag, W. Delle, N. Kirch, H. Nickel, K. Reinhart, E. Ziermann, Results of the visual in-pile inspection of the inner graphite reflector of the AVR, *Specialists' meeting on graphite component structural design, JAERI Tokai (Japan),* Vienna, 8-9-1986, International Atomic Energy Agency, 1986.

[10] W. Delle, Zum Bestrahlungsverhalten des Reflektorgraphits im AVR, ARS/AMT der Firma Sigri Elektrographit GmbH, Berichte der KFA Jülich, IRW-TN-43/83, 1983.

[11] R.E. Nightingale, Nuclear graphite, Academic press, New York and London, 1962.

[12] B. Bisplinghoff, M. Lochny, J. Fachinger, H. and Brücher, Radiochemical characterization of graphite from Jülich experimental reactor (AVR), *Nuclear Energy,* **39** [5], 311, 2000.

[13] C. Marnet, M. Wimmers, Decommissioning of the AVR reactor, concept for the total dismantling, *Technical committee meeting on technologies for gas cooled reactor decommissioning, fuel storage and waste disposal*, Vienna (Austria), 8-9-1997, 17, International Atomic Energy Agency, 1997.

[14] I.F. White, G.M. Smith, L.J. Saunders, Assessment of management modes for graphite from reactor decommissioning, Nuclear Science and Technology/Contract No DE-D-001-UK, 1984.

[15] R. Takahashi, M. Toyahara, S. Maruki, H. Ueda, T. Yamamoto, Investigation of morphology and impurity of nuclear-grade graphite, and leaching mechanism of carbon-14, 176, *IIAEA Technical Committee Meeting on "Nuclear Graphite Waste Management", held from 18-20 October 1999 in Manchester, United Kingdom*, 2004.

[16] R.P. Bush, G.M. Smith, I.F. White, Carbon-14 waste management, Nuclear science and technology, EUR 8749, Luxemburg: Office for Official Publications of the european communities, 1984.

[17] H. Scharf, Das System Cäsium-Graphit im Temperaturbereich 500-1000°C, Dissertation, KFA Jülich, 1969.

[18] R.J. Printz, U. Quade, J. Wahl, Packaging requirements for graphite and carbon from the decommissioning of the AVR in consideration of the German final disposal regulations, *Technical committee meeting on technologies for gas cooled reactor decommissioning, fuel storage and waste disposal. Juelich (Germany)* , Vienna (Austria), 8-9-1997, 275, International Atomic Energy Agency, 1997.

[19] S. Mrowec, Defects and diffusion in solids, Amsterdam-Oxford-New York, 1980.

[20] R.S. Sach, W.J. Williams, The diffusion of ^{14}C in nuclear graphite, *Carbon,* **12**, 425, 1974.

[21] B.F. Myers, W.E. Bell, Berichte der General Atomic Company, GA-A 13168, 1974.

[22] K. Hayashi, K. Fukuda, Diffusion coefficient of fission products in the UO_2 kernel and pyrocarbon layer of BISO-coated fuel particles, *Journal of Nuclear Materials,* **174**, 35, 1990.

[23] W. Schenk, A. Naoumidis, H. Nickel, The behaviour of spherical HTR fuel elements under accident conditions, *Journal of Nuclear Materials,* **124**, 25, 1984.

[24] E. Zimmer, B.G. Brodda, H. Kirchner, K. Kroth, Combustion of HTR fuel: fission product release and dissolution of plutonium contained in the ash, *Journal of Nuclear Materials,* **131**, 261, 1985.

[25] K. Iwamoto, The escape behaviour of non-gaseous fission products recoiled into graphite, *Journal of Nuclear Materials,* **29**, 285, 1969.

[26] J. Wörner, W. Botzem, S.D. Preston, Heat treatment of graphite and resulting tritium emissions, *IAEA Technical Committee Meeting on "Nuclear Graphite Waste Management", held from 18-20 October 1999 in Manchester, United Kingdom*, 1999.

[27] Fischer P.G., Verhalten von Tritium in Reaktorgraphiten, Berichte der KFA Jülich, Jül-1238, 1975.

[28] V.J. Malka, R. Raitz von Frentz, Adsorption und Desorption von Tritium an Graphit, Berichte der KFA Jülich, Jül-1497, Kernforschungsanlage Jülich, 1978.

[29] K. Ashida, K. Watanabe, Diffusion constants of tritium in graphites and compensation effect, *Journal of Nuclear Materials,* **183**, 89, 1991.

[30] M. Saeki, Effects of pyrolytic carbon structure on diffusivity of tritium, *Journal of Nuclear Materials,* **131**, 32, 1985.

[31] J.J. Guiroy, Graphite waste incineration in a fluidized bed, *Specialists meeting on graphite moderator lifecycle behaviour. Bath (United Kingdom).* 193, 1995.

[32] D. Bradbury, J.B. Mason, Pyrolysis and its potential use in nuclear graphite disposal, *Nuclear Energy,* **39** [5], 305, 2000.

[33] Schmidt P.C., Alternativen zur Verminderung der C-14-Emission bei der Wiederaufarbeitung von HTR-Brennelementen, Berichte der KFA Jülich, Jül-1567, 1979.

[34] J.G. Brown, P.D. Glynn, Kinetic dissolution of carbonates and Mn oxides in acidic water: measurement of in situ field rates and reactive transport modeling, *Applied Geochemistry,* **18** [8], 1225, 2003.

[35] O.S. Pokrovsky, J. Schott, Processes at the magnesium-bearing carbonates solution interface. II. Kinetics and mechanism of magnesite dissolution, *Geochimica et Cosmochimica Acta,* **63** [6], 881, 1999.

[36] Gray W.J., A study of the oxidation of graphite in liquid water for radioactive waste storage application, *Radioactive Waste Management,* **3** [2], 137, 1982.

[37] L.J. Hofer, E. Sterling, J.T. McCartney, Structure of the carbon deposited from carbon monoxide on iron, cobalt and nickel, *Journal of Physical Chemistry,* **59**, 1153, 1955.

[38] P.L. Walker, J.F. Rakszawski, G.R. Imperial, Carbon formation from carbon monoxide-hydrogen mixtures over iron catalysts. II. Rates of carbon formation, *Journal of Physical Chemistry,* **63**, 140, 1959.

[39] C. Marnet, G. Ivens, E. Ziermann, The AVR power-plant in its last year of operation, *Energy,* **16** [1-2], 71, 1991.

[40] J. Fassbender, E. Münch, D. Nutbohm, G. Thamm, Die gegenwärtige und zukünftige Nutzung der Forschungsreaktoren FRJ-1 (MERLIN) and FRJ-2 (DIDO) der Kernforschungsanlage Jülich, Berichte der KFA Jülich, 1973.

[41] G. Ramos, B.M.U. Scherzer, Radiation damage, trapping and release of deuterium in diamond and HOPG-graphite, *Nuclear Instruments & Methods in Physics Research Section B-Beam Interactions with Materials and Atoms,* **174** [3], 329, 2001.

[42] H. Yamagishi, N. Wakayama, H. Itoh, K. Sacasai, Measurement of neutron flux in the AVR, Berichte der KFA Jülich, JUEL-2467, 1991.

[43] Gmelin Handbuch der Annorganischen Chemie, Vol. 7, Verlag Chemie GmbH, Weinheimlbergstraße, 1966.

[44] T. Fakunaga, K. Itoh, S. Orimo, M. Aoki, H. Fujii, Location of deuterium atoms absorbed in nanocrystalline graphite prepared by mechanical alloying, *Alloys and Compounds,* **327**, 224, 2001.

[45] H. Atsumi, Hydrogen retention in graphite and carbon materials under a fusion reactor environment, *Journal of Nuclear Materials,* **313-316**, 543, 2003.

[46] H. Atsumi, K. Tauchi, Hydrogen absorption and transport in graphite materials, *Journal of Alloys and Compounds,* **356**, 705, 2003.

[47] S.L. Kanashenko, A.E. Gorodetsky, V.N. Chernikov, A.V. Markin, A.P. Zakharov, B.L. Doyle, W.R. Wampler, Hydrogen adsorption on and solubility in graphites, *Journal of Nuclear Materials,* **233-237**, 1207, 1996.

[48] D.M. Chen, T. Ichikawa, H. Fujii, N. Ogita, M. Udagawa, Y. Kitano, E. Tanabe, Unusual hydrogen absorption properties in graphite mechanically milled under various hydrogen pressures up to 6 MPa, *Alloys and Compounds,* **354**, L5, 2003.

[49] B.T. Kelly, Physics of graphite, Applied Science Publishers, London, 1981.

[50] G. DiCola, H.J. Matzke, *Nuclear Instruments & Methods,* **57**, 341, 1967.

[51] R.A. Causey, T.S. Elleman, K. Verghese, Hydrogen diffusion and solubility in pyrolitic carbon, *Carbon,* **17**, 323, 1979.

[52] R.C. Bansal, J.B. Donnet, F. Stoeckli, Active carbon, Vol. XIV, NY: Dekker, New-York, 1988.

[53] A. Dandekar, R.T.K. Baker, M.A. Vannice, Characterization of activated carbon, graphitized carbon fibers and synthetic diamond powder using TPD and DRIFTS, *Carbon,* **36** [12], 1821, 1998.

[54] S. Grigull, R. Behrisch, S. Parascandola, Nitrogen implantation into carbon: retention, release and target-erosion processes, *Journal of Nuclear Materials,* **275** [2], 158, 1999.

[55] J. Roth, W. Möller, Ion induced selfdiffusion of carbon, *Nuclear Instruments & Methods in Physics Research Section B-Beam Interactions with Materials and Atoms,* **13**, 409, 1986.

[56] B. Söder, J. Roth, W. Möller, The influence of the grain size on the mobility of irradiation induced self-interstitials in graphite, *Nuclear Instruments & Methods in Physics Research Section B-Beam Interactions with Materials and Atoms*, **32**, 160, 1988.

[57] B. Bisplinghoff, AVR-Analytik Ergebnissbericht, 2000.

[58] S. Maischak, J. Fachinger, G. Linse, R. Enge, W. Schädlich, α-,β- und γ-spektrometrische Untersuchungen an Graphitproben der Thermuschen Säule II des FRJ-1, 2001.

8 Appendix

Table 13. Tritium and ^{14}C release from Merlin graphite massive sample, 870°C, argon

M_0, g	Inventory ^{3}H, Bq	Inventory ^{14}C, Bq				
1.3644	20782	536				
Time hours	**^{3}H as triated H_2O Bq**	**^{3}H as triated H_2 Bq**	**Mass loss g**	**Time hours**	**^{14}C Bq**	**Mass loss g**
0.16	100	79	2.29E-05	0.16	–	2.29E-05
0.83	210	167	1.18E-04	0.83	–	1.18E-04
2.16	302	252	3.09E-04	2.16	–	3.09E-04
3.41	351	291	4.89E-04	3.41	13.2	4.89E-04
4.66	382	305	6.68E-04	4.66	12.3	6.68E-04
6.16	428	339	8.82E-04	6.16	14.0	8.82E-04
7.16	465	374	1.03E-03	7.16	16.0	1.03E-03
8.15	488	394	1.17E-03	8.15	19.4	1.17E-03
9.32	501	415	1.34E-03	9.32	18.7	1.34E-03
10.57	535	417	1.51E-03	10.57	19.3	1.51E-03
13.00	576	445	1.86E-03	13.00	25.2	1.86E-03
14.89	604	473	2.13E-03	14.89	26.1	2.13E-03
16.89	639	498	2.42E-03	16.89	28.1	2.42E-03
18.14	652	508	2.60E-03	18.14	29.1	2.60E-03

Table 14. Tritium and ^{14}C release from Merlin graphite powder sample, 970°C, argon

M_0, g	Inventory ^{3}H, Bq	Inventory ^{14}C, Bq				
0.4023	3704	235				
Time hours	**^{3}H as triated H_2O Bq**	**^{3}H as triated H_2 Bq**	**Mass loss g**	**Time hours**	**^{14}C Bq**	**Mass loss g**
0.67	90	30	4.91E-05	0.67	–	4.91E-05
1.08	124	47	7.98E-05	1.08	–	7.98E-05
1.67	143	55	1.23E-04	1.67	–	1.23E-04
3.00	204	70	2.21E-04	3.00	–	2.21E-04
4.25	240	80	3.13E-04	4.25	–	3.13E-04
5.17	263	87	3.80E-04	5.17	–	3.80E-04
6.17	275	93	4.54E-04	6.17	–	4.54E-04
7.17	293	95	5.28E-04	7.17	6.1	5.28E-04
8.17	306	100	6.01E-04	8.17	5.7	6.01E-04
9.00	319	104	6.63E-04	9.00	6.0	6.63E-04

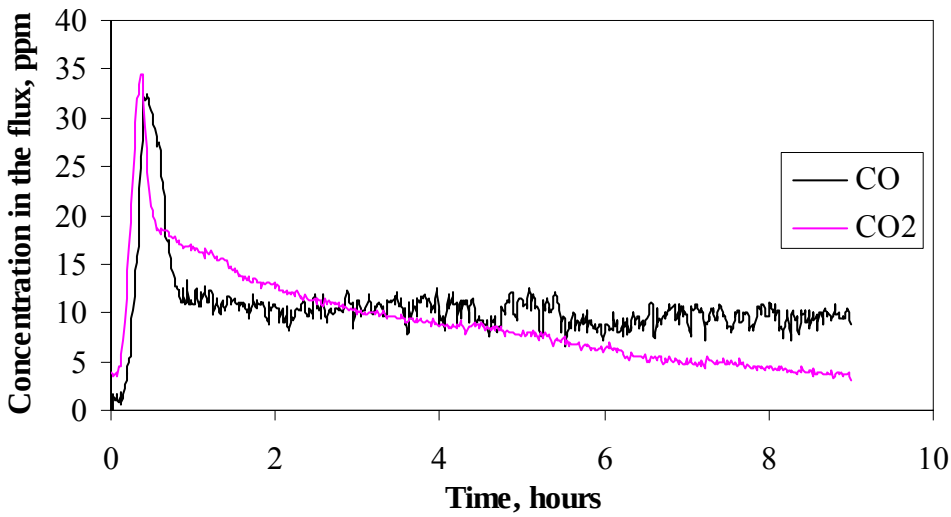

Figure 28. CO and CO_2 concentration in the outlet of carrier gas, Merlin graphite powder sample, 970°C, argon

Table 15. Tritium and ^{14}C release from Merlin graphite powder sample, 1050°C, argon

M_0, g	Inventory ^{3}H, Bq	Inventory ^{14}C, Bq
0.15	1487	89.6

Time hours	^{3}H as triated H_2O Bq	^{3}H as triated H_2 Bq	Mass loss g	Time hours	^{14}C Bq	Mass loss g
0.33	32	48	1.14E-04	0.83	–	1.14E-04
0.82	42	98	1.80E-04	1.32	–	1.80E-04
1.33	55	129	2.51E-04	1.83	–	2.51E-04
1.82	76	145	3.17E-04	2.32	–	3.17E-04
2.35	95	157	3.90E-04	2.85	3.4	3.90E-04
3.83	124	192	5.93E-04	4.33	4.5	5.93E-04
5.83	164	234	8.66E-04	6.33	5.9	8.66E-04
7.83	201	250	1.14E-03	8.33	7.3	1.14E-03
9.42	232	263	1.37E-03	9.92	10.0	1.37E-03
10.92	258	282	–	10.92	–	–
11.97	267	300	1.49E-03	11.97	14.8	1.49E-03
13.18	275	318	1.64E-03	13.18	17.1	1.64E-03
13.98	283	330	1.91E-03	13.98	16.9	1.91E-03
14.92	291	341	2.04E-03	14.92	18.3	2.04E-03

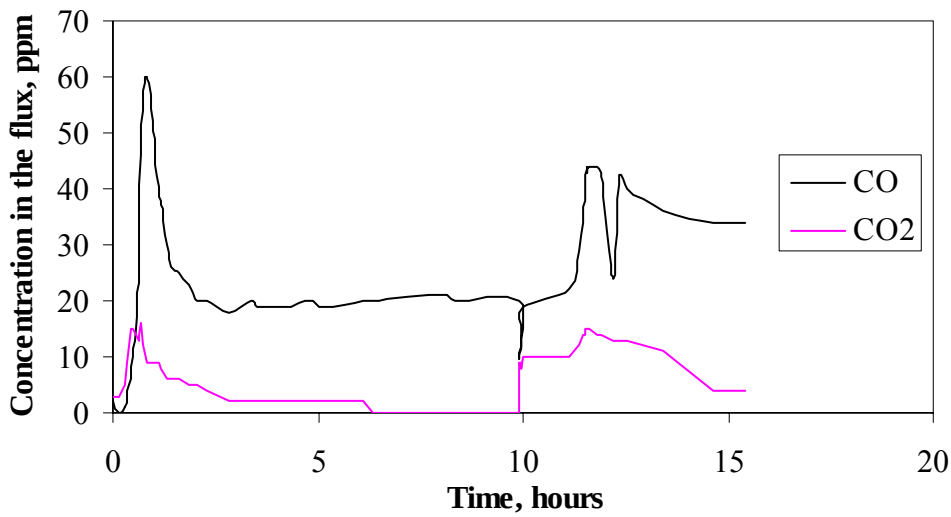

Figure 29. CO and CO_2 concentration in the outlet of carrier gas, Merlin graphite powder sample, 1050°C, argon

Table 16. Tritium and ^{14}C release from Merlin graphite massive sample, 1060°C, argon

M_0, g	Inventory ^{3}H, Bq	Inventory ^{14}C, Bq
0.9116	11446	531

Time hours	^{3}H as triated H_2O Bq	^{3}H as triated H_2 Bq	Mass loss g	Time hours	^{14}C Bq	Mass loss g
0.50	372	373	1.36E-04	0.50	–	1.36E-04
1.00	611	727	2.71E-04	1.00	9.2	2.71E-04
1.50	748	965	4.06E-04	1.50	12.7	4.06E-04
2.17	869	1142	5.86E-04	2.17	16.4	5.86E-04
3.34	1032	1393	9.01E-04	3.34	23.2	9.01E-04
4.84	1202	1636	1.31E-03	4.84	30.6	1.31E-03
5.92	1294	1807	1.60E-03	5.92	36.8	1.60E-03
7.99	1426	1981	2.16E-03	7.99	41.5	2.16E-03
11.24	1610	2202	3.03E-03	11.24	50.8	3.03E-03
13.40	1698	2331	3.62E-03	13.40	56.8	3.62E-03

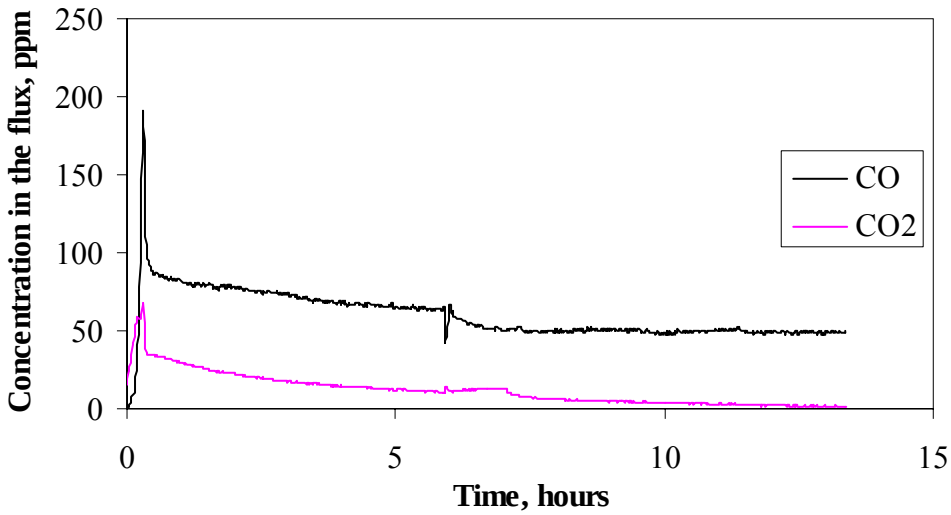

Figure 30. CO and CO_2 concentration in the outlet of carrier gas, Merlin graphite massive sample, 1060°C, argon

Table 17. Tritium and ^{14}C release from AVR graphite powder sample, 1060°C, argon

M_0, g	Inventory ^{3}H, Bq	Inventory ^{14}C, Bq
0.213	363649	25249

Time hours	^{3}H as triated H_2O Bq	^{3}H as triated H_2 Bq	Mass loss g	Time hours	^{14}C Bq	Mass loss g
0.66	11648	12824	1.17E-04	0.66	91	1.17E-04
1.67	23807	20901	2.94E-04	1.67	383	2.94E-04
2.67	29675	23096	4.70E-04	2.67	631	4.70E-04
3.67	34066	24977	6.46E-04	3.67	847	6.46E-04
4.67	37782	26377	8.23E-04	4.67	1032	8.23E-04
6.67	44163	29403	1.18E-03	6.67	1339	1.18E-03
7.83	47026	30294	1.38E-03	7.83	1522	1.38E-03
10.01	52096	32299	1.77E-03	10.01	1851	1.77E-03
11.01	54260	33229	1.94E-03	11.01	1969	1.94E-03
12.51	56641	34480	2.21E-03	12.51	2143	2.21E-03
14.01	59787	35450	2.47E-03	14.01	2317	2.47E-03
15.01	61573	36276	2.65E-03	15.01	2533	2.65E-03

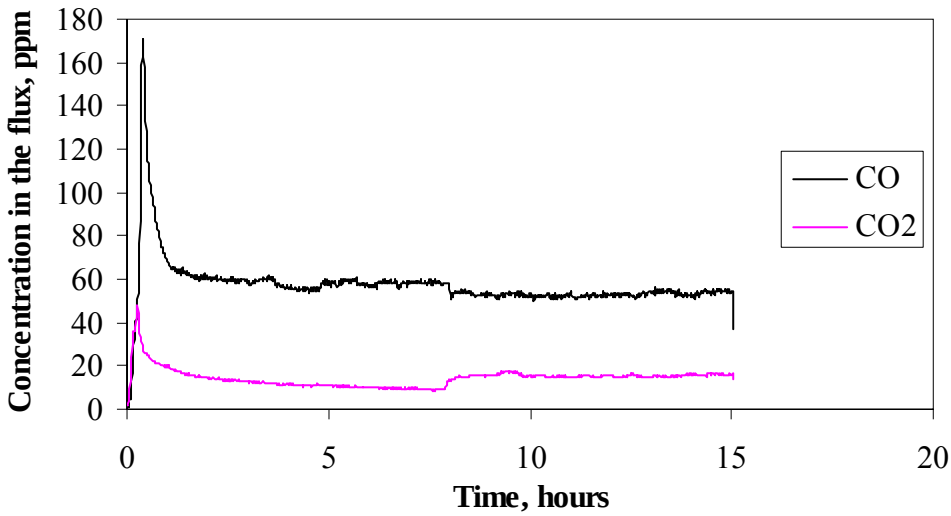

Figure 31. CO and CO_2 concentration in the outlet of carrier gas, AVR graphite powder sample, 1060°C, argon

Table 18. Tritium and ^{14}C release from Merlin graphite powder sample, 960°C, p_{H2O} 7.4 kPa, flow rate 80 ml/min

M_0, g	Inventory ^{3}H, Bq	Inventory ^{14}C, Bq				
0.2262	2411	117				
Time hours	**^{3}H as triated H_2O Bq**	**^{3}H as triated H_2 Bq**	**Mass loss g**	**Time hours**	**^{14}C Bq**	**Mass loss g**
0.25	153	66	1.96E-04	0.25	–	1.96E-04
0.58	204	136	4.57E-04	0.58	–	4.57E-04
1.33	309	260	1.05E-03	1.33	–	1.05E-03
2.50	364	374	1.96E-03	2.50	7.1	1.96E-03
3.50	429	460	2.74E-03	3.50	7.7	2.74E-03
4.58	488	555	3.59E-03	4.58	9.7	3.59E-03
5.33	538	–	4.18E-03	5.33	11.6	4.18E-03
6.42	572	635	5.03E-03	6.42	14.3	5.03E-03
7.42	582	708	5.81E-03	7.42	16.2	5.81E-03
8.25	610	754	6.47E-03	8.25	18.0	6.47E-03
9.42	671	871	7.38E-03	9.42	20.3	7.38E-03

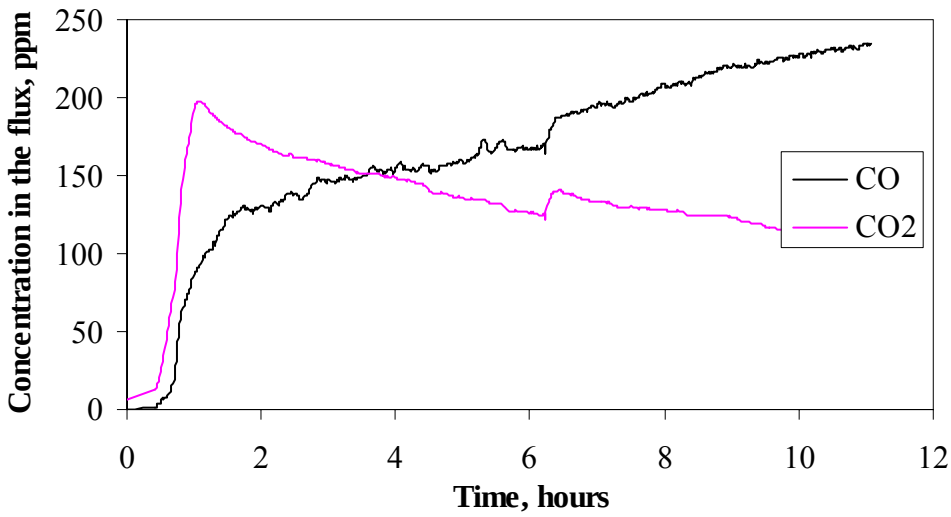

Figure 32. CO and CO_2 concentration in the outlet of carrier gas

Table 19. Tritium and ^{14}C release from Merlin graphite powder sample, 960°C, p_{H2O} 7.4 kPa, flow rate 660 ml/min

M_0, g	Inventory ^{3}H, Bq	Inventory ^{14}C, Bq
0.249	2824	190

Time hours	^{3}H as triated H_2O Bq	^{3}H as triated H_2 Bq	Mass loss g	Time hours	^{14}C Bq	Mass loss g
0.34	255	205	5.24E-04	0.67	–	1.04E-03
0.51	380	277	7.80E-04	1.17	14.3	1.81E-03
0.67	437	327	1.04E-03	2.42	25.2	3.73E-03
1.17	568	447	1.81E-03	3.67	29.1	5.65E-03
1.67	647	555	2.57E-03	4.67	35.3	7.19E-03
2.42	724	652	3.73E-03	5.67	42.8	8.73E-03
3.67	913	815	5.65E-03	6.51	44.6	1.00E-02
6.51	933	1026	1.00E-02	–	–	–

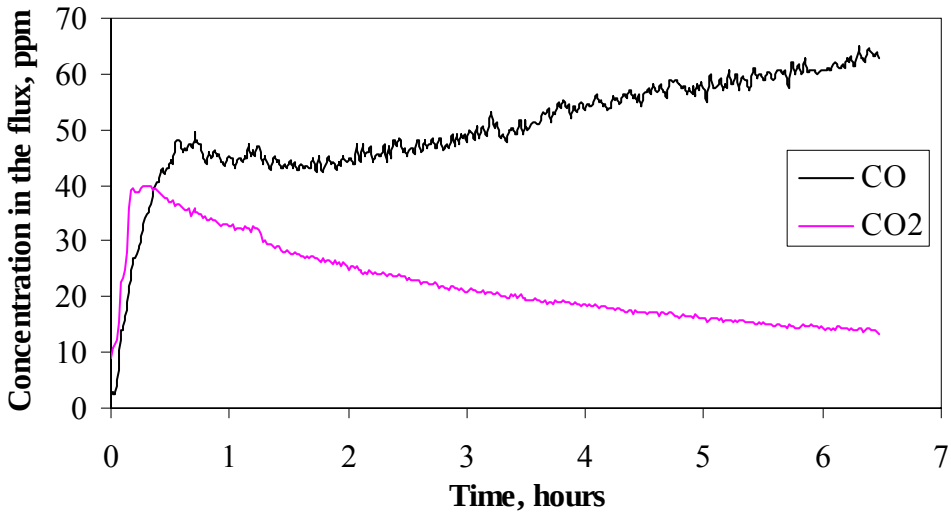

Figure 33. CO and CO_2 concentration in the outlet of carrier gas, Merlin graphite powder sample, 960°C, p_{H2O} 7.4 kPa, flow rate 660 ml/min

Table 20. Tritium and ^{14}C release from Merlin graphite massive sample, 1060°C, p_{H2O} 2.3kPa

M_0, g	Inventory ^{3}H, Bq	Inventory ^{14}C, Bq
0.446	9604	295

Time hours	^{3}H as triated H_2O Bq	^{3}H as triated H_2 Bq	Mass loss g	Time hours	^{14}C Bq	Mass loss g
0.66	22	448	7.89E-03	0.66	20	7.89E-03
0.74	164	1068	8.81E-03	0.82	30	9.76E-03
1.07	604	2033	1.27E-02	1.41	48	1.68E-02
2.41	2190	4610	2.87E-02	2.41	77	2.87E-02
3.41	3294	5994	4.06E-02	3.41	96	4.06E-02
4.41	4293	6914	5.25E-02	4.41	117	5.25E-02
5.52	5011	7789	6.57E-02	5.41	129	6.45E-02
7.09	5895	8682	8.44E-02	6.91	147	8.22E-02
8.24	6157	9038	9.81E-02	8.41	164	1.00E-01
10.07	6302	9383	1.20E-01	10.07	181	1.20E-01
11.41	6372	9498	1.36E-01	11.41	193	1.36E-01
12.94	6435	9498	1.54E-01	12.74	205	1.52E-01
14.74	6371	9658	1.75E-01	16.24	227	1.93E-01
16.24	6338	9577	1.93E-01	17.74	234	2.11E-01
17.74	6327	9577	2.11E-01	18.99	242	2.26E-01
18.99	6277	9550	2.26E-01	20.14	247	2.40E-01
20.14	6277	9550	2.40E-01	21.23	251	2.53E-01
21.23	6277	9550	2.53E-01	22.64	260	2.70E-01
22.64	6277	9550	2.70E-01	24.14	257	2.88E-01
25.24	6277	9550	3.01E-01	25.24	259	3.01E-01

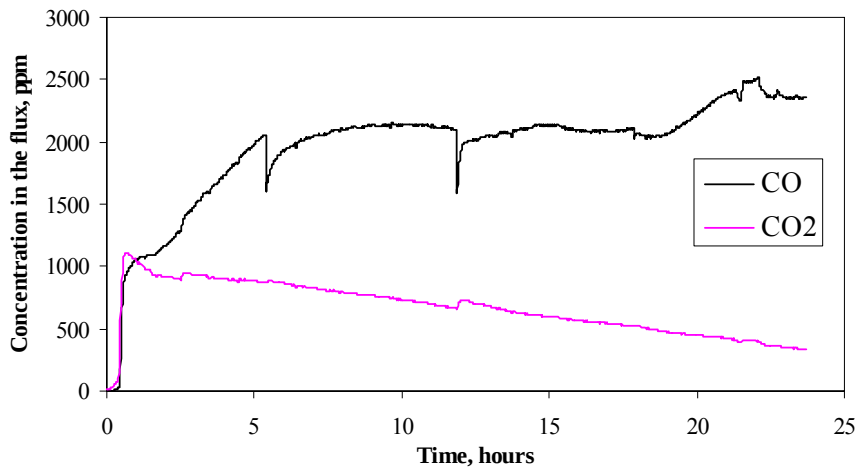

Figure 34. CO and CO_2 concentration in the outlet of carrier gas, from Merlin graphite massive sample, 1060°C, p_{H2O} 2.3kPa

Table 21. Tritium and ^{14}C release from Merlin graphite powder sample, 1050°C, p_{H2O} 2.3 kPa

M_0, g	Inventory ^{3}H, Bq	Inventory ^{14}C, Bq
0.439	3380	262

Time hours	^{3}H as triated H_2O Bq	^{3}H as triated H_2 Bq	Mass loss g	Time hours	^{14}C Bq	Mass loss g
0.73	11	257	7.73E-03	0.73	9.6	7.73E-03
0.98	52	398	1.04E-02	0.98	10.5	1.04E-02
1.56	238	608	1.66E-02	1.56	18.3	1.66E-02
2.39	408	779	2.54E-02	2.39	28.2	2.54E-02
3.39	625	926	3.61E-02	3.39	39.5	3.61E-02
4.48	843	1040	4.76E-02	4.48	51.7	4.76E-02
5.48	1017	1105	5.82E-02	5.48	60.7	5.82E-02
6.14	1178	1152	6.53E-02	6.14	70.1	6.53E-02
7.41	1701	1214	7.97E-02	7.41	83.0	7.97E-02
8.41	1746	1251	8.93E-02	8.41	90.4	8.93E-02
9.41	1764	1302	1.00E-01	9.41	96.7	1.00E-01

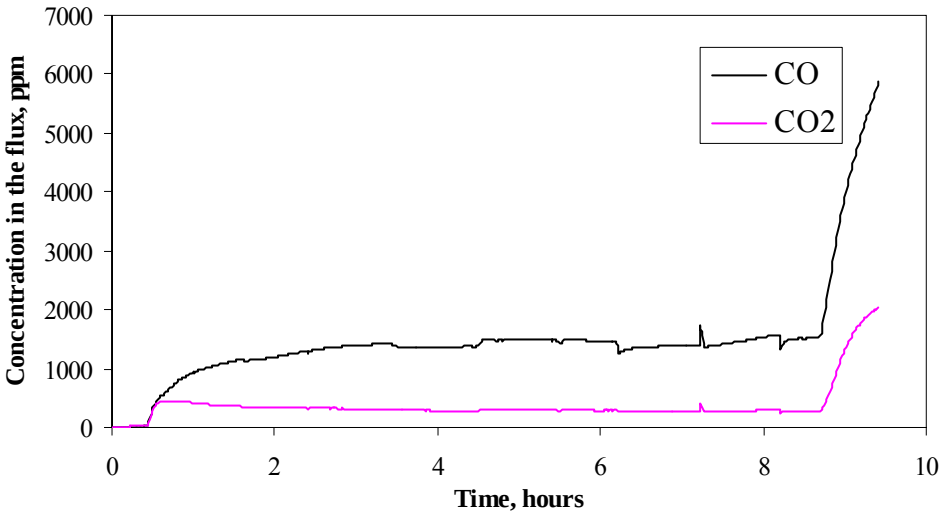

Figure 35. CO and CO_2 concentration in the outlet of carrier gas, Merlin graphite powder sample, 1050°C, p_{H2O} 2.3 kPa

Table 22. Tritium and ^{14}C release from Merlin graphite powder sample, 1060°C, p_{H2O} 7.4 kPa, flow rate 660 ml/min

M_0, g	Inventory ^{3}H, Bq	Inventory ^{14}C, Bq				
0.239	1993	152				
Time hours	**^{3}H as triated H_2O Bq**	**^{3}H as triated H_2 Bq**	**Mass loss g**	**Time hours**	**^{14}C Bq**	**Mass loss g**
0.17	265	188	1.57E-03	0.17	5.8	1.57E-03
0.33	399	281	3.14E-03	0.33	9.5	3.14E-03
0.50	466	343	4.71E-03	0.50	12.9	4.71E-03
1.00	621	466	9.42E-03	1.00	18.9	9.42E-03
2.00	786	607	1.88E-02	2.00	29.7	1.88E-02
5.00	940	778	4.71E-02	3.00	42.5	2.83E-02
6.00	918	802	5.65E-02	4.00	50.2	3.77E-02
7.00	911	820	6.60E-02	5.00	59.4	4.71E-02
8.00	909	834	7.54E-02	8.00	94.9	7.54E-02
9.00	–	–	–	9.00	100.7	8.48E-02
10.00	–	–	–	10.00	107.6	9.42E-02
11.00	–	–	–	11.00	113.0	1.04E-01

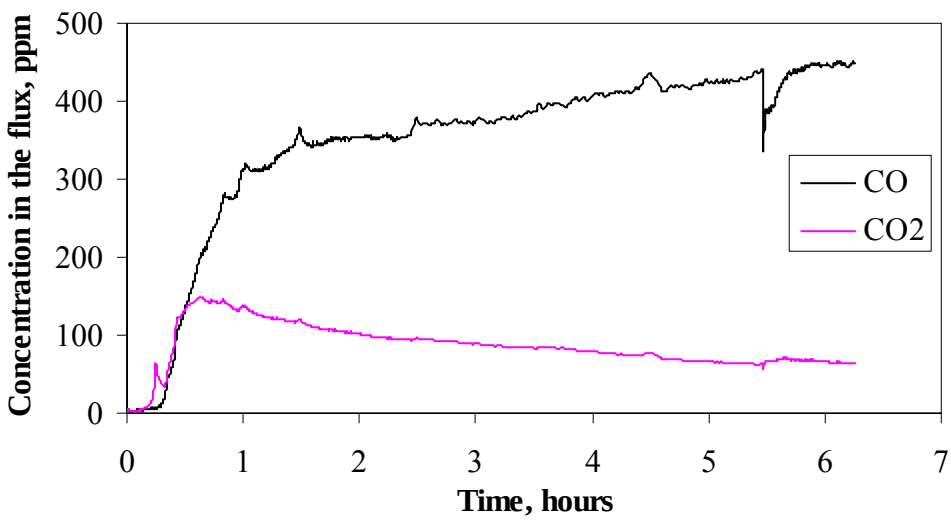

Figure 36. CO and CO_2 concentration in the outlet of carrier gas, Merlin graphite powder sample, 1060°C, p_{H2O} 7.4 kPa, flow rate 660 ml/min

Table 23. Tritium and ^{14}C release from AVR graphite powder sample, 1060°C, 2.3 kPa

M_0, g	Inventory ^{3}H, Bq	Inventory ^{14}C, Bq			
0.087	142276	11414			
Time, hours	**^{3}H, as triated water, Bq**	**^{3}H, as triated hydrogen, Bq**	**Time, hours**	**^{14}C, Bq**	**Mass loss, g**
0.91	13076	3068	0.91	472	8.22E-04
1.91	20279	5074	1.91	947	1.73E-03
2.91	24386	6702	2.91	1348	2.63E-03
3.91	28930	7930	3.91	1748	3.53E-03
4.91	30175	8841	4.91	2063	4.44E-03
5.91	32931	9449	5.91	2293	5.34E-03
6.91	35064	10466	6.91	2577	6.24E-03
7.91	36441	11174	7.91	2806	7.15E-03
9.49	38555	12314	9.49	3214	8.58E-03
10.32	43063	12957	10.32	3461	9.33E-03
11.32	43288	13755	11.32	3665	1.03E-02
12.99	44921	14601	12.99	3934	1.17E-02
13.99	45638	15529	13.99	4167	1.26E-02
14.99	46225	16358	14.99	4346	1.35E-02
15.82	46977	16700	15.82	4421	1.43E-02

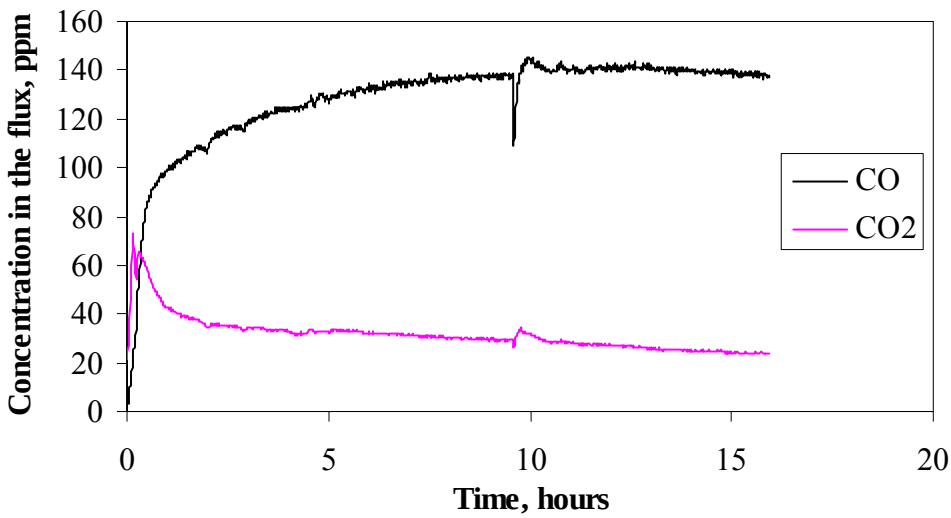

Figure 37. CO and CO_2 concentration in the outlet of carrier gas, AVR graphite powder sample, 1060°C, 2.3 kPa

Table 24. Tritium and ^{14}C release from AVR graphite powder sample, 1060°C, p_{H2O} 31 kPa

M_0, g	Inventory ^{3}H, Bq	Inventory ^{14}C, Bq				
0.0726	107057	10006				
Time hours	**^{3}H as triated H_2O Bq**	**^{3}H as triated H_2 Bq**	**Mass loss g**	**Time hours**	**^{14}C Bq**	**Mass loss g**
0.54	1520	3068	2.72E-04	0.54	98	2.72E-04
1.54	20470	5074	4.37E-03	1.54	1299	4.37E-03
2.54	29279	6702	8.83E-03	2.54	2089	8.83E-03
4.54	44605	7930	1.74E-02	4.54	3678	1.74E-02
6.54	55536	8841	2.50E-02	6.54	4597	2.50E-02
8.00	61480	9449	3.00E-02	8.00	5354	3.00E-02
10.50	65808	10466	3.69E-02	10.50	6146	3.69E-02
11.60	66333	11174	3.95E-02	11.60	6431	3.95E-02
12.60	68332	12314	4.16E-02	12.60	6529	4.16E-02
13.10	68125	12957	4.26E-02	13.10	6861	4.26E-02

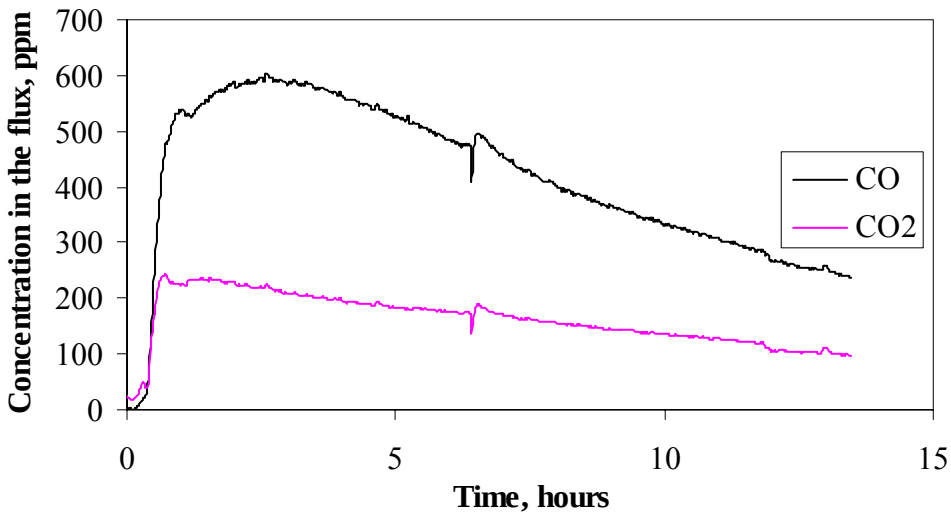

Figure 38. CO and CO_2 concentration in the outlet of carrier gas, AVR graphite powder sample, 1060°C, p_{H2O} 31 kPa

Table 25. γ-analysis of AVR graphite

	Activity, Bq/g						
Sample Nr.	**^{60}Co**	**^{133}Ba**	**^{134}Cs**	**^{137}Cs**	**^{152}Eu**	**^{154}Eu**	**^{155}Eu**
1	12040	1425	169	3623	<30	632	166
2	14030	1331	202	2421	<30	664	189
3	10693	1431	190	2204	<30	518	148
4	11620	1477	111	4065	<30	522	151
5	13050	1420	230	2252	<30	605	154
6	11921	1385	165	2285	<30	517	138
7	16610	1585	110	2810	<30	564	142
8	17210	1400	180	3157	<30	650	176
Average	13397	1432	170	2852		584	158
Reported data*	18913	653	122	711	80	621	183

* - [57] sample S-GR-5 Nr.1 corrected to time

Table 26. γ-analysis of Merlin graphite

	Activity, Bq/g						
Sample Nr.	**^{60}Co**	**^{133}Ba**	**^{134}Cs**	**^{137}Cs**	**^{152}Eu**	**^{154}Eu**	**^{155}Eu**
1	413	–	–	0.14	625	56	–
2	569	–	–	0.21	654	61	–
Reported data*	654	410	–	–	820	70	4

* - [58] sample TS10 corrected to time